

## PHAT: PHoto-z Accuracy Testing<sup>★</sup>

H. Hildebrandt<sup>1</sup>, S. Arnouts<sup>2</sup>, P. Capak<sup>3</sup>, L. A. Moustakas<sup>4</sup>, C. Wolf<sup>5</sup>, F. B. Abdalla<sup>6</sup>, R. J. Assef<sup>7</sup>, M. Banerji<sup>8</sup>, N. Benítez<sup>9</sup>, G. B. Brammer<sup>10</sup>, T. Budavári<sup>11</sup>, S. Carliles<sup>12</sup>, D. Coe<sup>4</sup>, T. Dahmen<sup>13</sup>, R. Feldmann<sup>14</sup>, D. Gerdes<sup>15</sup>, B. Gillis<sup>16</sup>, O. Ilbert<sup>17</sup>, R. Kotulla<sup>18,19</sup>, O. Lahav<sup>6</sup>, I. H. Li<sup>20</sup>, J.-M. Miralles<sup>21</sup>, N. Purger<sup>22</sup>, S. Schmidt<sup>23</sup>, and J. Singal<sup>24</sup>

<sup>1</sup> Leiden Observatory, Leiden University, Niels Bohrweg 2, 2333CA Leiden, The Netherlands  
e-mail: [hendrik@strw.leidenuniv.nl](mailto:hendrik@strw.leidenuniv.nl)

<sup>2</sup> Canada-France-Hawaii Telescope Corporation, Kamuela, HI 96743, USA

<sup>3</sup> Spitzer Science Center, 314-6, California Institute of Technology, 1201 E. California Blvd, Pasadena, CA, 91125, USA

<sup>4</sup> Jet Propulsion Laboratory, California Institute of Technology, MS 169-327, Pasadena, CA 91109, USA

<sup>5</sup> Department of Physics, University of Oxford, DWB, Keble Road, Oxford, OX1 3RH, UK

<sup>6</sup> Department of Physics and Astronomy, University College London, Gower Street, London WC1E 6BT, UK

<sup>7</sup> Department of Astronomy, The Ohio State University, 4055 McPherson Lab, 140 W. 18th Avenue, Columbus, OH 43210, USA

<sup>8</sup> Institute of Astronomy, University of Cambridge, Madingley Road, Cambridge, CB3 0HA, UK

<sup>9</sup> Instituto de Astrofísica de Andalucía (CSIC), Apdo. 3044, 18008 Granada, Spain

<sup>10</sup> Department of Astronomy, Yale University, New Haven, CT 06520-8101, USA

<sup>11</sup> Department of Physics and Astronomy, Johns Hopkins University, 3400 North Charles Street, Baltimore, MD 21218, USA

<sup>12</sup> Department of Computer Science, Johns Hopkins University, 3400 North Charles Street, Baltimore, MD 21218, USA

<sup>13</sup> Space Telescope Science Institute, 3700 San Martin Drive, Baltimore, MD 21218, USA

<sup>14</sup> Department of Physics, Institute of Astronomy, ETH Zürich, Wolfgang-Pauli-Strasse 16, 8093 Zürich, Switzerland

<sup>15</sup> Department of Physics, University of Michigan, Ann Arbor, Michigan 48109, USA

<sup>16</sup> Department of Physics and Astronomy, University of Waterloo, 200 University Avenue West, Waterloo, Ontario, N2L 3G1, Canada

<sup>17</sup> Laboratoire d’Astrophysique de Marseille, CNRS-Université d’Aix-Marseille, 38 rue Frédéric Joliot-Curie, 13388 Marseille Cedex 13, France

<sup>18</sup> Centre for Astrophysics Research, University of Hertfordshire, College Lane, Hatfield AL10 9AB, UK

<sup>19</sup> Department of Astronomy, University of Wisconsin-Madison, 475 N Charter St., Madison, WI 53706, USA

<sup>20</sup> Centre for Astrophysics & Supercomputing, Swinburne University of Technology, PO Box 218, Hawthorn, VIC 3122, Australia

<sup>21</sup> Institut d’Estudis Andorrans, Avda Rocafort 21–23, AD600 Sant Julià de Lòria, Andorra

<sup>22</sup> Department of Physics of Complex Systems, Eötvös Loránd University, Pf. 32, 1518 Budapest, Hungary

<sup>23</sup> Physics Department, University of California, 1 Shields Avenue, Davis, CA 95616, USA

<sup>24</sup> Kavli Institute for Particle Astrophysics and Cosmology, SLAC National Accelerator Laboratory, Menlo Park, CA 94025, USA

Received 29 April 2010 / Accepted 23 July 2010

### ABSTRACT

**Context.** Photometric redshifts (photo- $z$ ’s) have become an essential tool in extragalactic astronomy. Many current and upcoming observing programmes require great accuracy of photo- $z$ ’s to reach their scientific goals.

**Aims.** Here we introduce PHAT, the PHoto- $z$  Accuracy Testing programme, an international initiative to test and compare different methods of photo- $z$  estimation.

**Methods.** Two different test environments are set up, one (PHAT0) based on simulations to test the basic functionality of the different photo- $z$  codes, and another one (PHAT1) based on data from the GOODS survey including 18-band photometry and  $\sim 2000$  spectroscopic redshifts.

**Results.** The accuracy of the different methods is expressed and ranked by the global photo- $z$  bias, scatter, and outlier rates. While most methods agree very well on PHAT0 there are differences in the handling of the Lyman- $\alpha$  forest for higher redshifts. Furthermore, different methods produce photo- $z$  scatters that can differ by up to a factor of two even in this idealised case. A larger spread in accuracy is found for PHAT1. Few methods benefit from the addition of mid-IR photometry. The accuracy of the other methods is unaffected or suffers when IRAC data are included. Remaining biases and systematic effects can be explained by shortcomings in the different template sets (especially in the mid-IR) and the use of priors on the one hand and an insufficient training set on the other hand. Some strategies to overcome these problems are identified by comparing the methods in detail. Scatters of 4–8% in  $\Delta z/(1+z)$  were obtained, consistent with other studies. However, somewhat larger outlier rates ( $>7.5\%$  with  $\Delta z/(1+z) > 0.15$ ;  $>4.5\%$  after cleaning) are found for all codes that can only partly be explained by AGN or issues in the photometry or the spec- $z$  catalogue. Some outliers were probably missed in comparisons of photo- $z$ ’s to other, less complete spectroscopic surveys in the past. There is a general trend that empirical codes produce smaller biases than template-based codes.

**Conclusions.** The systematic, quantitative comparison of different photo- $z$  codes presented here is a snapshot of the current state-of-the-art of photo- $z$  estimation and sets a standard for the assessment of photo- $z$  accuracy in the future. The rather large outlier rates reported here for PHAT1 on real data should be investigated further since they are most probably also present (and possibly hidden) in many other studies. The test data sets are publicly available and can be used to compare new, upcoming methods to established ones and help in guiding future photo- $z$  method development.

**Key words.** techniques: photometric – galaxies: distances and redshifts – galaxies: photometry – cosmology: observations – methods: data analysis

## 1. Introduction

The estimation of redshifts from photometry alone is an old idea (Baum 1962; Puschell et al. 1982; Koo 1985; Loh & Spillar 1986; Connolly et al. 1995). It has come a long way from being a rarely used technique for special kinds of objects to a major tool now widely used for a multitude of observational programmes.

Not only can this photometric redshift (photo- $z$ ) approach yield redshifts of fainter objects than accessible by spectroscopy, but also the efficiency in terms of the number of objects with redshift estimates per unit telescope time is largely increased. These two properties make photo- $z$ 's extremely attractive for observing programmes depending on redshifts for a large number of faint galaxies if these redshifts do not have to be as precise as spectroscopic redshifts (spec- $z$ 's).

Still the requirements on the accuracy of photo- $z$ 's for upcoming surveys are formidable. Photo- $z$ 's are essential in constraining dark energy (DE) by weak gravitational lensing and can be used for other DE probes such as galaxy clustering, supernovae of type Ia, and the mass function of galaxy clusters as well (Albrecht et al. 2006; Peacock et al. 2006). Surveys of galaxy formation and evolution also depend on photo- $z$ 's to study these processes as a function of environment and to probe to fainter levels than with spectroscopy alone. To fully exploit the power of these huge, future data sets, photo- $z$ 's with a very low level of residual systematics are needed (e.g. Huterer et al. 2006).

There are many aspects which influence the performance of photo- $z$ 's. The choice of an observing strategy sets the theoretical limit for the accuracy. Choosing the filters and distributing the available observing time over the different filters to reach certain depths can have a great impact on photo- $z$ 's. Accurate photometric calibration is of great importance as well as the removal of effects of the different point-spread-function (PSF) in the different bands. Varying column densities of galactic dust over the survey area have to be accounted for before a photo- $z$  code can be expected to perform at its best.

Here we would like to ignore all these effects as much as possible and concentrate on the last link in the chain, the photo- $z$  methods themselves. It is clear that the two regimes – data and method – cannot be separated cleanly because there are connections between the two. For example, it is highly likely that one method of photo- $z$  estimation will perform better than a second method on one particular data set while the situation may well be reversed on a different data set. Whenever such a situation arises in the following we will try to alert the reader to that.

The methodology behind photo- $z$ 's is developing fast with ever more complex methods yielding results of increasing accuracy. In this context it is important to set a standard to compare the different methods to each other in order to make quantitative statements about their differences and to take a snapshot of today's state-of-the-art. Such comparisons and rankings can then be used to identify the most promising approaches and to concentrate on their further improvement.

In this paper we present an international initiative named PHAT (PHoto- $z$  Accuracy Testing)<sup>1</sup> which was initiated to carry out such a quantitative comparison. A very similar initiative has been carried out for shape measurement algorithms in the Shear

TEsting Program (STEP; Heymans et al. 2006; Massey et al. 2007) and led to important improvements in the methodology of measuring galaxy shapes for weak gravitational lensing applications. Similar but much more limited blind tests of photo- $z$ 's have been performed by Hogg et al. (1998) on spectroscopic data from the Keck telescope on the *Hubble* Deep Field (HDF), by Hildebrandt et al. (2008) on spectroscopic data from the VIMOS VLT Deep Survey (VVDS; Le Fèvre et al. 2004) and the FORS Deep Field (FDF; Noll et al. 2004), and by Abdalla et al. (2008b) on the sample of Luminous Red Galaxies from the SDSS-DR6.

In the framework of PHAT we provide standardised test environments to the photo- $z$  community which consist of simulated or observed photometric catalogues alongside with additional material like filter curves, SED templates, and training sets. These data sets can be used in a blind (or semi-blind, i.e. with support of a training set) test by the participants to estimate redshifts with their favourite codes. Two such test steps have been carried out so far. The first one called PHAT0 is based on a highly idealised simulation representing an easy case to test the most basic elements of photo- $z$  estimation and to identify possible low-level discrepancies between the methods. The second test called PHAT1 is based on real data originating from the Great Observatories Origins Deep Survey (GOODS, Giavalisco et al. 2004) representing a much more complex environment pushing photo- $z$  codes to their limits and revealing more systematic difficulties.

PHAT was conceived as an open competition. The test data sets are publicly available over the PHAT website and all major photo- $z$  groups in the astronomical community were informed of the initiative via email. Furthermore, PHAT was advertised on several meetings and workshops to increase its visibility. The photo- $z$  codes presented here were not selected by the PHAT coordinators but reflect the interest of the community in such a competition. This strategy led to an impressive feedback of 21 participants submitting results obtained with 17 different photo- $z$  codes. After a large number of results was collected for each test data set, the results of all codes were published on the PHAT website. But the test data sets are still kept blind (i.e. the individual redshifts are retained) to allow further participants to meet the same conditions.

First we shortly summarise every photo- $z$  method that was used within PHAT (Sect. 2). Then in Sects. 3 and 4 the motivation behind the tests, the data sets, and the results are described in detail for PHAT0 and PHAT1, respectively. In Sect. 5 we conclude and give an outlook to future activities within PHAT. We use AB magnitudes throughout.

## 2. Methods

In the following we describe the different methods that were used to estimate photo- $z$ 's from the catalogues presented in Sects. 3 and 4. A summary of the methods can also be found in Table 1 together with the three-letter acronyms that are used in the remainder of the paper to identify the codes. The third small letter indicates whether the code belongs to the empirical codes (-e), which are trained on the colours<sup>2</sup> of a sub-sample of objects with accurate redshift estimates (e.g. spec- $z$ 's), or to the codes fitting SED templates to the observed photometry (-t). It should be noted that this distinction is somewhat fuzzy. A number of

\* Based on observations obtained with the Hubble Space Telescope, the Spitzer Space Telescope, the Keck Observatory, the Kitt Peak National Observatory, the Subaru Telescope, the Palomar Observatory, and the University of Hawaii 2.2-m telescope.

<sup>1</sup> [http://www.astro.caltech.edu/twiki\\_phat/bin/view/Main/WebHome](http://www.astro.caltech.edu/twiki_phat/bin/view/Main/WebHome)

<sup>2</sup> Most empirical codes offer the flexibility of using also any other photometric observable like e.g. size, concentration, or surface brightness. Since we only use magnitudes in PHAT we skip this detail in the remainder of Sect. 2.

**Table 1.** Methods used for photo-z estimation within PHAT.

Acronym	Participant	Code	Reference	Public
BP-t	Coe, D.	BPZ, Bayesian Photometric Redshifts	Benítez (2000); Coe et al. (2006)	✓ <sup>a</sup>
BP2-t	Benítez, N.	BPZ, Bayesian Photometric Redshifts	Benítez (2000); Benítez 2010 (in prep.)	✓ <sup>a</sup>
EA-t	Brammer, G.	EAZY, Easy and Accurate Redshifts from Yale	Brammer et al. (2008)	✓ <sup>b</sup>
GA-t	Kotulla, R.	GALEV, GALaxy EVolution	Kotulla et al. (2009)	✓ <sup>c</sup>
GO-t	Dahlen, T.	GOODZ	Dahlen et al. (2005, 2007)	
HY-t	Miralles, J.-M.	Hyperz	Bolzonella et al. (2000)	✓ <sup>d</sup>
KR-t	Schmidt, S.	Kernelz, Kernel Regression	Schmidt & Brewer (in prep.)	
LP-t	Arnouts, S.	Le Phare	Ilbert et al. (2006)	✓ <sup>e</sup>
	Ilbert, O.			
LR-t	Assef, R.	LRT, Low-Resolution Spectral Templates	Assef et al. (2008, 2010)	✓ <sup>f</sup>
PT-t	Purger, N.	Template Repair	Adelman-McCarthy et al. (2007)	✓ <sup>g</sup>
ZE-t	Feldmann, R.	ZEBRA, Zurich Extragalactic Bayesian Redshift Analyzer	Feldmann et al. (2006)	✓ <sup>h</sup>
ZE2-t	Gillis, B.	ZEBRA, Zurich Extragalactic Bayesian Redshift Analyzer	Feldmann et al. (2006)	✓ <sup>h</sup>
AN-e	Abdalla, F.	ANNz, Artificial Neural Network	Collister & Lahav (2004)	✓ <sup>i</sup>
	Banerji, M.			
DT-e	Gerdes, D.	BDT, Boosted Decision Trees	Gerdes et al. (2010)	
EC-e	Wolf, C.	Empirical $\chi^2$	Wolf (2009)	
PN-e	Purger, N.	Nearest-Neighbour Fit	Abazajian et al. (2009)	✓ <sup>g</sup>
PO-e	Li, I. H.	Polynomial Fit	Li & Yee (2008)	
RT-e	Carliles, S.	Regression Trees	Carliles et al. (2010)	✓ <sup>j</sup>
SN-e	Singal, J.	Neural Network	—	✓ <sup>k</sup>

**Notes.** <sup>(a)</sup> <http://acs.pha.jhu.edu/~txitxo/>; version 1.99.3 used for PHAT: <http://www.its.caltech.edu/~coe/BPZ/> <sup>(b)</sup> <http://www.astro.yale.edu/eazy/> <sup>(c)</sup> <http://www.galev.org/> <sup>(d)</sup> <http://webast.ast.obs-mip.fr/hyperz/> <sup>(e)</sup> <http://www.cfht.hawaii.edu/~arnouts/lephare.html> <sup>(f)</sup> <http://www.astronomy.ohio-state.edu/~rjassem/lrt/> <sup>(g)</sup> <http://skyserver.elte.hu/PhotoZ/> <sup>(h)</sup> <http://www.exp-astro.phys.ethz.ch/ZEBRA/> <sup>(i)</sup> <http://www.homepages.ucl.ac.uk/~ucapola/annz.html> <sup>(j)</sup> <http://www.sdss.jhu.edu/~carliles/photoZ/> <sup>(k)</sup> <http://www.slac.stanford.edu/~jacks/>

codes include ingredients from both regimes. We just keep this terminology because it has been widely used in the literature. For a more rigorous description of the underlying concepts in photo-z methods and their common properties see Budavári (2009).

Note that the descriptions of the different template sets of the template SED fitting codes in the following subsections only apply to PHAT1. For PHAT0 the template set was provided and it was used by every participant with a template-based code.

## 2.1. BPZ (BP-t)

BPZ (Bayesian Photo-z's; Benítez 2000) introduced the use of Bayesian inference and priors to photometric redshift estimation. The code uses a prior  $P(z, T | m_0)$  which gives the likelihood that given an apparent magnitude  $m_0$ , a galaxy would have redshift  $z$  and SED type  $T$ . As an example of how the prior works, bright objects and ellipticals are assumed unlikely to be at high redshift. For each galaxy, this information is combined (in a Bayesian manner) with the likelihood  $P(C | z, T)$  of observing the galaxy colours  $C$  for each redshift and SED pair, yielding the final  $P(z, T | C, m_0)$ . By marginalising over  $T$ ,  $P(z)$  is obtained along with the most likely redshift  $z_b$  and its uncertainties. For the PHAT tests, BPZ version 1.99.3 is used, a slightly updated version of that used in the Coe et al. (2006) UDF analysis.

- **Templates:** the Coe et al. (2006) SED templates are used with BPZ, which include a CWW+SB SED template set (similar to that used in PHAT0 with Kinney et al.'s SB1 replaced by SB3) as introduced in Benítez (2000) and re-calibrated by Benítez et al. (2004) plus two younger starburst templates from Bruzual & Charlot (2003) added in Coe et al. (2006). Note that the empirical CWW+SB templates as well as the

synthetic BC03 templates include emission lines. No dust extinction was added to the BC03 templates. Between each of the eight adjacent templates two interpolated templates are added, for a total of 22 templates. Beyond 25 600 Å, the majority of the templates are undefined and must be extrapolated. Thus it cannot be expected that these templates provide good fits to IRAC photometry of low redshift objects;

- **Prior:** for PHAT0, a flat prior is used. The prior was calculated by Benítez (2000) based on objects with spec-z in the CFRS (Lilly et al. 1995) and HDF-N (Williams et al. 1996). It was shown to yield results superior to the “flat” prior implicitly assumed by maximum likelihood (or “frequentist”) methods;
- **Training:** no training with the model-z's/spec-z's was performed.

## 2.2. BPZ (BP2-t)

BPZ is run on PHAT1 a second time with a different template set and additional training.

- **Templates:** the second library (Benítez 2010, in preparation) uses as starting point a set of 6 templates from PEGASE (Fioc & Rocca-Volmerange 1997) selected to be similar to the Coe et al. (2006) templates. This library is further calibrated using the FIREWORKS photometry and spectroscopic redshifts from Wuyts et al. (2008). Note that these templates include emission lines and dust extinction;
- **Prior:** same as BP-t;
- **Training:** the templates are compared to the photometry of the spec-z training set and new zero points are estimated, as in Coe et al. (2006). We also measure the amount of excess

scatter in the predicted vs measured colours compared with that expected from the catalogue photometric errors and typical template uncertainties (Brammer et al. 2008). This excess scatter is included in the photo-z estimation as a zero point uncertainty.

### 2.3. EAZY (EA-t)

EAZY (Brammer et al. 2008) is a template-fitting code designed to produce un-biased photometric redshift estimates for deep multi-wavelength surveys that lack representative calibration samples with spectroscopic redshifts.

- *Templates*: EAZY uses a unique template set derived using the non-negative matrix factorisation algorithm (Sha et al. 2007; Blanton & Roweis 2007) trained on synthetic photometry from the semi-analytic light-cone produced by De Lucia & Blaizot (2007). These templates can be considered the principal component spectra of all galaxies at  $0 < z < 4$  in the light-cone, allowing for subtle differences between local and high-redshift galaxy samples. EAZY is able to reproduce complex star-formation histories by fitting non-negative linear combinations of the templates. The templates include emission lines following the prescription of Ilbert et al. (2009);
- *Template error function*: template mismatch is addressed with a “template error function”, which assigns lower weights at rest-frame wavelengths where the template calibration is uncertain or where the templates are not expected to fully reproduce observed galaxy colours. This feature is particularly important when using mid-IR (IRAC) photometry, which samples wavelengths where the observed emission can be dominated by non-stellar (i.e. dust) sources not included in the templates;
- *Prior*: EAZY adopts a prior equal to the normalised redshift distribution of galaxies in the De Lucia & Blaizot (2007) semi-analytic light-cone at a given apparent  $R$  or  $K$  magnitude. This is akin to a luminosity prior under the assumption that the light-cone reasonably reproduces the galaxy luminosity function;
- *Training*: no training with the model- $z$ ’s/spec- $z$ ’s was performed.

### 2.4. GALEV and GAZELLE (GA-t)

GAZELLE (Kotulla & Fritze 2009, Kotulla, in preparation) is based on a  $\chi^2$  minimisation algorithm to compare the observed SEDs to a large library of GALEV evolutionary synthesis models (Kotulla et al. 2009). GAZELLE also accounts for inherent uncertainties in the model grid, e.g. due to uncertainties in the stellar evolution data and stellar spectral libraries, by assuming a 0.1 mag uncertainty in all filters.

- *Templates*: GALEV includes a full suite of emission lines (Anders & Fritze 2003), a detailed treatment of the attenuation due to intergalactic HI (Madau 1995) and optionally a chemical evolution model. This combination allows to not only estimate photometric redshifts, but at the same time physical parameters (stellar masses, star formation rates, etc.) for each galaxy in a consistent manner. Masses and mass-dependent parameters are computed by scaling model values with the scaling factor derived from matching the overall normalisation of the template fluxes relative to the observed fluxes. For the PHAT1 run the model

grid included 5 undisturbed models for E and Sa-Sd type galaxies supplemented with a set of 21 models encountering a strong starburst at galaxy ages of 0.5 to 10 Gyr, followed by subsequent post-starburst phases. All models assume star formation to begin at  $z = 8$ ; for the undisturbed models a chemically consistent evolution (see Kotulla & Fritze 2009, for details) is chosen, for the burst models a metallicity fixed to half the solar value is used. All templates include the full evolution from the onset of star formation until the present day and the Calzetti et al. (2000) dust extinction description is chosen. Emission lines are included as well;

- *Filter weighting*: to avoid complications at wavelengths beyond the rest-frame  $K$ -band where dust emission becomes increasingly important, only filters that cover the rest-frame  $K$ -band or shorter wavelengths are included, effectively ignoring some of the Spitzer filters at low-redshift;
- *Prior*: no prior is included that might affect the resulting redshift distribution;
- *Training*: no training with the model- $z$ ’s/spec- $z$ ’s was performed.

### 2.5. GOODZ (GO-t)

The GOODZ code (Dahlen et al. 2010, in preparation) is a developed version of the code used by Dahlen et al. (2005, 2007) to calculate photometric redshifts in the GOODS-S. The code is based on the template fitting method and allows the inclusion of Bayesian priors based on the expected shape of the galaxy luminosity function. Similar to this investigation, GOODZ uses the four empirical templates from Coleman et al. (1980) and two templates from (Kinney et al. 1996, their templates SB2 and SB3). The code also uses available spectroscopic redshifts to correct for offsets between fluxes extracted in different filters or instruments. Such offsets may be significant when combining data from different instruments with varying PSF or pixel-scales and may uncorrected lead to increased scatter or biases in the photometric redshifts. The spectroscopic redshifts are also used to adjust the input set of template SEDs using a method similar to Ilbert et al. (2006).

- *Templates*: GOODZ is only run on PHAT0 so that no individual template set is associated with this code;
- *Prior*: no prior was used;
- *Training*: no training with the model- $z$ ’s was performed.

### 2.6. Hyperz (HY-t)

Hyperz is a publicly available code based on SED templates fitting using a standard  $\chi^2$  minimisation method. The codes uses the observed fluxes of an object in a set of given filters and compares them with the theoretical fluxes of galaxies in the same filters obtained from template spectra, either synthetic or empirical, taking into account the observational uncertainties but also the possible observational hidden effects such as reddening or IGM opacity. It computes not only a best-fit solution which minimises the differences, therefore a most probable photometric redshift, but also a full probability function as a function of redshift. The code and the method have been tested and described extensively in Bolzonella et al. (2000) and further practical description can be found in its users manual. Hyperz comes with a given set of templates, filters, reddening laws and Lyman forest modelling but can be easily adapted to use any kind of parameters that would fit the needs of the user. Its simplicity has brought Hyperz to be extensively used and tested since its

launch, and even to be used beyond the pure computation of photometric redshifts.

- *Templates*: Hyperz comes with two standard template sets, one based on the synthetic stellar population library of [Bruzual & Charlot \(1993\)](#) and the other one consisting of the four empirical templates from [Coleman et al. \(1980\)](#). For the PHAT1 test, the latter empirical library was chosen and it was supplemented with two starburst templates from [Kinney et al. \(1996\)](#) (templates from both libraries include emission lines). This set of six basic template was further enlarged by applying different amounts of extinction to the templates according to the [Calzetti et al. \(2000\)](#) dust extinction law;
- *Prior*: no prior was used;
- *Training*: no training with the model- $z$ 's/spec- $z$ 's was performed.

### 2.7. Kernelz (KR-t)

This method is a hybrid incorporating aspects of both template-based and empirical codes, though it is most similar in design to BPZ and other Bayesian methods. As in standard template-based codes model colours are computed for a set of galaxy SEDs at a set of fixed redshifts. However, then this grid of colours is treated as if they were individual galaxies. For each test galaxy the points are weighted by a factor that is akin to a Bayesian prior, accounting for the expected probability of seeing such a galaxy given the apparent magnitude and type of the test point. Redshifts are then estimated using kernel regression, constructing a weighted average redshift, with weights proportional to their proximity to the template points in colour space. The kernel bandwidth is chosen by cross-validation using the training set of galaxies with known redshifts. Results presented here represent code that is still in development. Details of the kernel regression method for both empirical and hybrid techniques will be described in Schmidt & Brewer (in prep.). A promising extension that improves the method by allowing for data adaptive kernels will be described in Udal'tsova & Schmidt (in prep.). A public release of the code is also in the works.

- *Templates*: because Kernelz was still in development when the results were submitted, simple templates from [Coleman et al. \(1980\)](#) and [Kinney et al. \(1996\)](#) (both of which include emission lines) with some extrapolation to IRAC wavelengths were used;
- *Prior*: an empirical prior trained on data from VVDS was used. In practice, this is very similar to the prior described in [Ilbert et al. \(2006\)](#);
- *Training*: the spectroscopic data was used to choose the kernel bandwidth alone, no tweaking of templates or zero points was performed.

### 2.8. Le Phare (LP-t)

The public code Le Phare ([Arnouts et al. 2002](#); [Ilbert et al. 2006](#)) is primarily dedicated to estimate photo- $z$ 's, but it can also be used to estimate physical parameters like stellar masses and infrared luminosities. Le Phare is based on a standard template fitting procedure. The templates are redshifted and integrated through the instrumental transmission curves. The opacity of the IGM is taken into account and internal extinction could be added as a free parameter to each galaxy. The photo- $z$ 's are obtained by comparing the modelled fluxes and the observed fluxes with a  $\chi^2$

merit function. A probability distribution function is associated to each photo- $z$ .

For the PHAT1 sample, we adopted a configuration similar to the one used in the COSMOS field ([Ilbert et al. 2009](#)):

- *Templates*: the set of templates was generated by [Polletta et al. \(2007\)](#) with the code GRASIL ([Silva et al. 1998](#)). The 9 galaxy templates of [Polletta et al. \(2007\)](#) include 3 SEDs of elliptical galaxies and 6 templates of spiral galaxies (S0, Sa, Sb, Sc, Sd, Sdm). Those were complemented with 12 additional blue templates generated with [Bruzual & Charlot \(2003\)](#). Four different dust extinction laws were applied ([Prevot et al. 1984](#); [Calzetti et al. 2000](#), and an additional bump at 2175 Å), depending on the considered template. Emission lines were added to the templates using relations between the UV continuum, the star formation rate and the emission line fluxes ([Kennicutt 1998](#));
- *Prior*: no prior on the redshift distribution was applied. However, no redshift solution which would produce a galaxy brighter than  $M(B) = -24$  was allowed. Such a prior would create catastrophic failure for some QSOs, but it was not explicitly intended to estimate photo- $z$ 's for QSOs (no AGN templates were included in this run), although the PHAT1 catalogue contains some (see below);
- *Training*: an automatic calibration of the zero-points was performed using the spec- $z$  sample. The calibration is obtained by comparing the observed and modelled fluxes ([Ilbert et al. 2006](#)). The calibration is done iteratively until convergence in the zero-points values is reached. This step helps in removing bias.

### 2.9. LRT (LR-t)

LRT (Low-Resolution Spectral Templates [Assef et al. 2008, 2010](#)) is a set of subroutines intended for estimating K-corrections and photometric redshifts using a basis of empirical low resolution SED templates (hence LRT) for galaxies and AGNs. In this basis, every galaxy is represented by a non-negative linear combination of three empirically determined SED templates that resemble an elliptical, an Sbc spiral and an Im irregular galaxy. Given the nature of the tests in the PHAT initiative, the AGN SED template was not used. For the PHAT0 testing phase, the LRT subroutines were modified to do a simple  $\chi^2$  minimisation to fit each template to the data separately rather than fitting a non-negative combination of them.

- *Templates*: the templates were derived from the extensive broad-band and spectroscopic observations of the NOAO Deep Wide-Field Survey ([Jannuzi & Dey 1999](#)) Boötes field and range in wavelength between 0.03 and 30  $\mu\text{m}$ . In the PHAT1 testing phase, the LRT subroutines were used with the SED templates derived in [Assef et al. \(2008\)](#) which have a shorter wavelength range (0.1–10  $\mu\text{m}$ ) than the newer versions presented in [Assef et al. \(2010\)](#). These newer SED templates also integrate an AGN component with variable extinction;
- *Prior*: for estimating photometric redshifts, the LRT subroutines also use a simple luminosity function prior, which is by default based on the  $R$ -band luminosity function of [Lin et al. \(1996\)](#);
- *Training*: no training with the model- $z$ 's/spec- $z$ 's was performed.

### 2.10. Purger (Template Repair) (PT-t)

Originated from the template-based method described in [Csabai et al. \(2003\)](#), this method uses synthetic colours calculated from the given spectral energy distribution templates. A common approach for template fitting is to take a small number of spectral templates T and choose the best fit by optimising the likelihood of the fit as a function of redshift, type, and luminosity,  $p(z, T, L)$ . Here a variant of this method is used that incorporates a continuous distribution of spectral templates, enabling the error function in redshift and type to be well defined.

- *Templates*: this code is only run on PHAT0 so that no individual template set is associated with this code;
- *Prior*: no prior was used;
- *Training*: no training with the model- $z$ 's was performed.

### 2.11. ZEBRA (ZE-t & ZE2-t)

ZEBRA (Zurich Extragalactic Bayesian Redshift Analyzer [Feldmann et al. 2006](#)) is a freely available, open source photometric redshift code based on a SED template-fitting approach. Built on top of a traditional Maximum Likelihood ansatz it introduces and combines several novel methods that help to improve the accuracy of photometric redshift estimates for galaxies and AGNs (see e.g. [Oesch et al. 2010](#); [Luo et al. 2010](#), for some recent applications). First, ZEBRA is able to detect and correct photometric offsets in the input catalogue. Second, ZEBRA can use spectroscopic redshifts on a small fraction of the photometric sample to iteratively correct the original set of input templates. This template correction step has been shown to be a crucial ingredient in decreasing the bias, the scatter, and the number of outliers in the redshift estimation (e.g. [Feldmann et al. 2006](#); [Mobasher et al. 2007](#)). Third, when run in Bayesian mode ZEBRA computes the prior in redshift-template space in a self-consistent manner from the input catalogues and the redshift-template likelihood functions. This prior is consequently used to derive the posterior probability distribution of each input object. Here, since ZEBRA participates only in PHAT0, it is run in its basic Maximum Likelihood mode and with the provided templates. The following set of parameters are used. The redshifts are allowed to vary in steps of 0.002 from 0 to 4. The filter bands are mildly smoothed using a top-hat filter with  $FWHM$  of 20 Å. Finally, the spectral flux densities weighted with photon energy, not photon counts, are computed using the  $-\text{flux-type} = 1$  option. For the ZE2-t runs the redshift stepping is reduced to 0.001 and no smoothing of the filter bands is performed.

- *Templates*: ZEBRA is only run on PHAT0 so that no individual template set is associated with this code;
- *Prior*: no prior was used;
- *Training*: no training with the model- $z$ 's was performed.

### 2.12. ANNz (AN-e)

ANNz ([Collister & Lahav 2004](#)) is an empirical photo- $z$  code based on artificial neural networks. Such a network is made up of several layers, each consisting of a number of nodes. The first layer receives the galaxy magnitudes as inputs, while the last layer outputs the estimated photometric redshift. The layers in between could consist of any number of nodes each. The nodes are inter-connected, and every connection carries a “weight”, which is a free parameter in the parametrisation. When a network is trained the weights of all node connections are determined by minimising a cost function  $E$ . To avoid an over-fitting,

every network is tested on a validation set of galaxies, whose spectroscopic redshifts are also known. The network with lowest value of  $E$  as calculated on the validation set is selected and the photometric sample is run through it for redshift estimation. An error bar is assigned to each photo- $z$  via a chain rule (see [Collister & Lahav 2004](#), for details). Neural networks have been used e.g. for estimation of photo- $z$ 's for the SDSS ([Collister et al. 2007](#); [Oyaizu et al. 2008](#); [Abdalla et al. 2008b](#)), as well as forecasts of photometric redshifts for future surveys like the Dark Energy Survey ([Banerji et al. 2008](#)) and Euclid ([Abdalla et al. 2008a](#)).

A neural network architecture of N:2N:2N:1 was used for the PHAT tests where N is the number of filters for which there are input magnitudes. Different architectures were tested, but this did not lead to any substantial improvement in the results. The choice of architecture is fully justified by tests done in [Firth et al. \(2003\)](#) and [Collister & Lahav \(2004\)](#).

### 2.13. BDT (DT-e)

The Boosted Decision Tree (BDT) algorithm ([Gerdes et al. 2010](#)) is a training-set-based method that combines an ensemble of weak classifiers into a single, powerful classifier. The spectroscopic training set is first divided into redshift bins whose width is approximately half the expected photo- $z$  resolution of the algorithm for the given sample. We have found that a finer binning choice does not improve the resolution. For each bin, a set of trees is trained intended to recognise as “signal” those galaxies whose redshift falls within the bin in question, and “background” those that fall more than  $2\sigma$  away from the signal bin, where  $\sigma$  is the iteratively-determined photo- $z$  resolution. As training variables we use the observed magnitudes in each band. The process of constructing an individual tree begins with a root node containing all the training galaxies. The root node is then split into two subsamples by placing a cut on the one variable that best separates the sample into signal and background. Each new node is subsequently split in this way until the nodes reach a certain minimum size. The result is a tree containing nodes with predominantly signal and predominantly background galaxies. The process of “boosting” iteratively repeats this process, giving higher weight to galaxies that were initially misclassified. The overall signal probability of a galaxy is then obtained by combining the classification output from approximately 50 trees in each photo- $z$  bin, where higher weight is given to trees with lower misclassification rates in the training set.

The method produces a photo- $z$  probability for each galaxy as a function of redshift. This method therefore yields not only an estimate of the best photo- $z$  and error, but a reconstruction of the full redshift PDF,  $P(z)$ . In [Gerdes et al. \(2010\)](#) it was shown that the BDT algorithm improves upon the default photo- $z$ 's in the SDSS spectroscopic sample, and that the PDFs yield a more accurate reconstruction of the redshift distribution  $N(z)$ .

### 2.14. Wolf (empirical $\chi^2$ ) (EC-e)

The method of [Wolf \(2009\)](#) derives PDFs from empirical models and is a subclass of kernel regression methods. It mimics a template-based  $\chi^2$ -technique with the main difference that an empirical dataset is used in place of the template grid. Each object in the empirical set contributes to the observed object with a quantified probability. The PDF of redshifts thus obtained can be used in its entirety or investigated for ambiguities. Here, it is just reduced to an expectation value and RMS in redshift. Any kernel

approach requires to choose a kernel function which also acts as a smoothing scale to the discrete empirical model grid. Here, we used a Gaussian kernel function with  $\sigma_m = 0^m 1$ . However, a  $\chi^2$ -method is correctly implemented if the kernel function applied to the model makes its density distribution match that of the observed sample (see the matched error scale in Sect. 6 of [Wolf 2009](#), for details). As a consequence, redshift distributions of object samples can be reconstructed potentially accurate within Poisson noise of the sample sizes, which would also imply no bias exceeding random noise.

### 2.15. Purger (nearest-neighbour Fit) (PN-e)

This empirical method compares the observed colours to the reference set. The estimation method first searches the colour space for the  $k$  nearest neighbours of every object in the estimation set (i.e. the galaxies for which we want to estimate redshift) and then estimates the redshift by fitting a local low order polynomial to these points. An improved version of this code is using a k-d tree index for fast nearest neighbour search ([Csabai et al. 2007](#)). It was used to calculate photometric redshifts for the SDSS Data Release 7 ([Abazajian et al. 2009](#)). The advantage of this method versus a template-based method might be the better estimation accuracy, but it cannot extrapolate, so the completeness of the reference set is crucial. For this reason, we have used the large training set available for the PHATO test.

The estimation was done using the large, simulated data set using 150 nearest neighbours. A small number of outliers was automatically excluded from the regression on the neighbour sets.

### 2.16. Li (polynomial) (PO-e)

This empirical photo- $z$  method is based on [Li & Yee \(2008\)](#), which uses a polynomial fit so that the galaxy redshift is expressed as the sum of its magnitudes and colours. Different from [Li & Yee \(2008\)](#) where the training set galaxies are divided into several fixed colour-magnitude cells, here the coefficients of the photo- $z$  polynomial are derived individually for each galaxy by choosing a subset of training set galaxies whose magnitudes and colours are closest to the input galaxy. They are chosen based on quadratically summed ranks of colour and magnitude differences between the training set galaxies and the input galaxy. All magnitudes and independent colours are used. Note that each training set galaxy has an equal weight in the fit. This may introduce a redshift bias to input galaxies near the edges of the colour-magnitude distributions. Therefore, a better approach would be to assign weights to the chosen training-set galaxies based on the inverse value of their final rank, but this has not been implemented for PHAT.

### 2.17. Carliles (regression trees) (RT-e)

The RT-e method by [Carliles et al. \(2010\)](#) is based on Random Forests which are an empirical, non-parametric regression technique. A Random Forest builds an ensemble average of randomised regression tree redshift estimates. Bootstrap samples are created by sampling from the training set with replacement, and each regression tree is trained on its own bootstrap sample. Given a new test object, each regression tree produces its own redshift estimate, and these estimates are averaged to yield the final Random Forest redshift estimate. This technique also results in Gaussian errors, and this behaviour has a strong theoretical

statistical explanation. Intuitively speaking, a given new galaxy can be considered to be drawn from the space of inputs (colours, magnitudes, etc.) by redshifts. This space is the event space, and for that new galaxy one can hypothesise the existence of a distribution over the event space, unique to that galaxy, which reflects the similarity of the new galaxy (minus the unknown redshift) to any given point in the event space. The Random Forest approximates this distribution per object, and the process results in easily computable per-object error parameter estimates.

For the PHAT tests a leaf size of 5 was chosen and 50 trees were used.

### 2.18. Singal (neural network) (SN-e)

The primary motivation for the development of this code was to treat additional available galaxy information beyond photometric data, for example shape parameters, on an equal footing with the photometric data (as it was done in e.g. [Collister & Lahav 2004](#); [Ball et al. 2004](#)). The package, although still undergoing modification, is a multi-layer perceptron neural network for the IDL environment. The IDL code can be relatively easily modified, and could in principle be optimised for a variety of input data situations. As training convergence is relatively slow in this network, it is most useful in situations where a robust training set is available from the outset.

As implemented here, the network has an input layer of neurons which accepts the magnitudes in each band. The input layer treats all input information on an equal footing, normalising across all objects in the training set so that the inputs for each neuron on the input layer are distributed between 0 and 1. There are two hidden layers of 30 neurons each, and an output layer with a single neuron obtaining a value between 0 and 1 which is a proxy for the estimated redshift, with the linear conversion defined during the training when the known redshifts of the training set are supplied subject to the conversion.

## 3. PHATO – a highly idealised simulation

### 3.1. Motivation

The lowest algorithmic level of the codes can be tested if the photometry is bias-free and everything except for the redshifts is provided. In this way the choice of template sets, the use of priors, etc. do not play a role and code-specific problems can be disentangled from other effects. To this end, simulations with synthetic photometry are set up with the LP-t photo- $z$  code (see Sect. 2.8).

### 3.2. Data set

In order to keep things simple PHATO is based on a very limited template set and a long wavelength baseline. A noise-free catalogue with accurate synthetic colours is provided as well as a catalogue with a low level of additional noise. Furthermore, we added a very large training set to ensure that also empirical photo- $z$  algorithms find an ideal environment. The ingredients are detailed in the following.

Everything but the redshifts for the test data set was revealed to the participants. In particular, the template set (Sect. 3.2.1) and the filter curves (Sect. 3.2.2) were provided, and details about the construction of the catalogues (Sects. 3.2.3 and 3.2.4; e.g. the used IGM recipe) were revealed. The participants were explicitly asked to use those ingredients if applicable to make their setup as comparable to the simulation setup as possible.

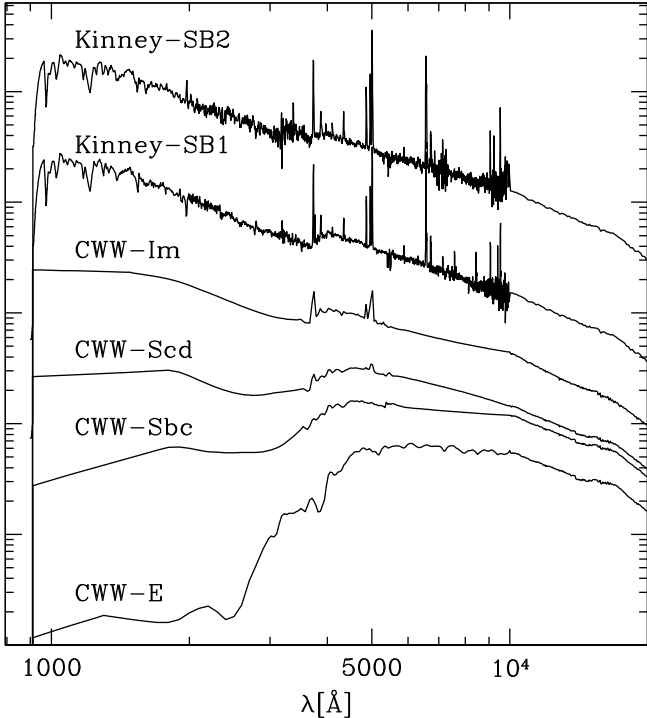


**Fig. 1.** Template set used for the PHAT0 test (arbitrary flux normalisation).

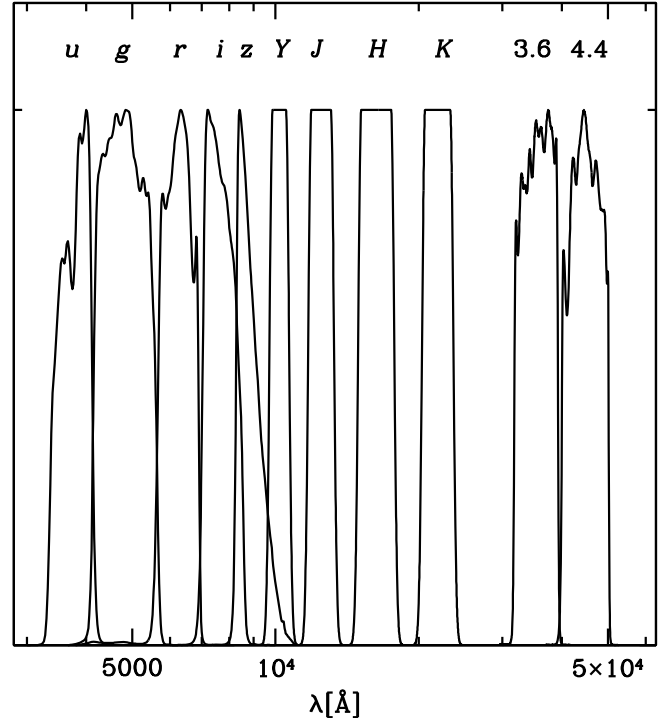


**Fig. 2.** Transmission curves of the filter set used for the PHAT0 test.

### 3.2.1. Template set

The empirical template set by [Coleman et al. \(1980\)](#) has been used extensively in different photo- $z$  studies. As in the case of LP-t ([Ilbert et al. 2006](#)) and BP-t ([Benítez 2000](#)) we decided to supplement this template set by two templates for starburst galaxies from [Kinney et al. \(1996\)](#). The template SEDs are displayed in Fig. 1.

It should be noted that the choice of the template set is not critical in this test because the template set is provided to the participants using template-based codes and the very large training set (see below) covers densely the whole SED-redshift space. This particular set is chosen here because it is one of the most widely used sets for photo- $z$ 's in its original, extended, and modified (re-calibrated) form. Participants using template-based codes were explicitly asked to use this particular template set for the PHAT0 test and switch off any priors within their codes.

### 3.2.2. Filter set

For the PHAT0 test we want to avoid systematic effects that can arise in photo- $z$ 's because of an insufficient coverage in wavelength. For example, colour-redshift degeneracies (see e.g. [Benítez 2000](#)) can occur between high- and low-redshift if infrared (IR) and/or ultraviolet (UV) bands are not available.

Thus, the filter set used here spans the whole range from near-UV to mid-IR (see Fig. 2). We choose the  $ugriz$ -bands from MEGACAM mounted at the CFHT ([Boulade et al. 2003](#)), the  $YJHK$ -bands of UKIDSS ([Lawrence et al. 2007](#)), and the two bluer bands of the IRAC camera mounted on the Spitzer Space Telescope ([Fazio et al. 2004](#)). Again this choice is not too critical since the filter curves are provided and one of the tests does not include any noise at all and the other one includes just a low level of noise in the photometry.

### 3.2.3. Noise-free catalogue

One of the most simple tests one can think of is to compare the redshift estimates of different codes for data with infinite signal-to-noise ( $S/N$ ) and thus perfect colours. In this way the agreement of the basic interpolation- and convolution-algorithms in template-based codes can be tested. Any differences found in such a basic test will probably propagate to more realistic setups.

We use the LP-t code as a reference to create such a catalogue evenly distributed over the six templates and over the redshift range  $0 < z < 4$  including the effect of absorption by the intergalactic medium (IGM) following the recipe by [Madau \(1995\)](#). The model redshifts were revealed to the participants for this test.

It should be noted that inaccurate redshift estimates from one of the codes only mean that this particular code does not agree perfectly with LP-t. Which of the two codes is inaccurate (or whether even both are inaccurate) cannot be decided with such a test.

### 3.2.4. Catalogue with noise

To study the influence of noise on the results, a more realistic catalogue is set up as well. We adopt a parametric form for the signal-to-noise as a function of magnitude which behaves as a power-law at bright magnitudes and an exponential at faint magnitudes. The transition regime is defined by the parameters  $(m_*, \text{err}_*)$ . At magnitude  $m \leq m_*$ , we adopt  $\text{err}(m) = 10^{0.4(\alpha_{\text{bright}}+1)(m-m_*)}$ , and at magnitude  $m \geq m_*$ , we use  $\text{err}(m) = \frac{\text{err}_*}{2.72} \cdot \exp(10^{\alpha_{\text{faint}}(m-m_*)})$ , where  $\alpha_{\text{bright}}$  and  $\alpha_{\text{faint}}$  are the slopes at bright and faint magnitudes respectively. The adopted values for each filter are reported in Table 2, while the behaviour of the Signal-to-Noise ( $S/N = 1.086/\text{err}$ ) for the different passbands is shown in Fig. 3 (colour coded from  $u$  band, in cyan to  $4.5 \mu\text{m}$ , in red). The noisy magnitudes are randomly drawn

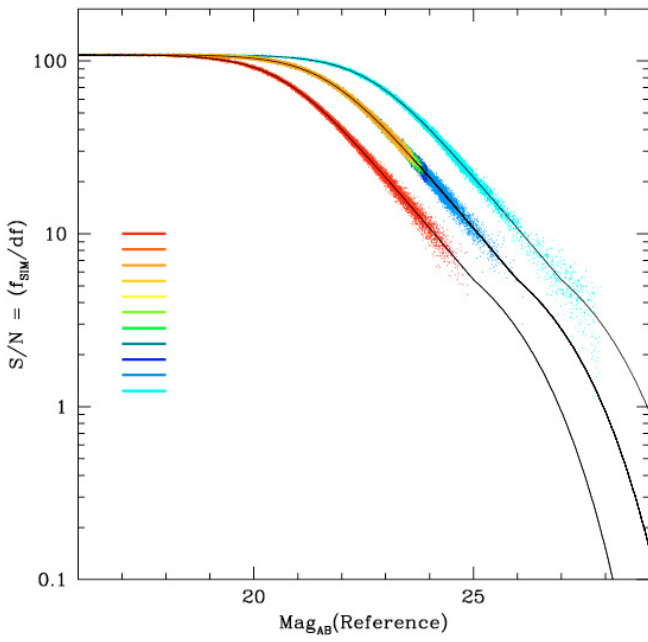


**Fig. 3.** Signal-to-noise model used for the PHAT0 test.

**Table 2.** Filters used for the PHAT0 test.

Filter	Instrument	$m_\star$	err $_\star$	$\alpha_{\text{bright}}$	$\alpha_{\text{faint}}$
$u$	MEGACAM@CFHT	27.0	0.2	-0.25	0.22
$g$	MEGACAM@CFHT	26.0	0.2	-0.25	0.22
$r$	MEGACAM@CFHT	26.0	0.2	-0.25	0.22
$i$	MEGACAM@CFHT	26.0	0.2	-0.25	0.22
$z$	MEGACAM@CFHT	26.0	0.2	-0.25	0.22
$Y$	WFCAM@UKIRT	26.0	0.2	-0.25	0.22
$J$	WFCAM@UKIRT	26.0	0.2	-0.25	0.22
$H$	WFCAM@UKIRT	26.0	0.2	-0.25	0.22
$K$	WFCAM@UKIRT	26.0	0.2	-0.25	0.22
$3.6 \mu\text{m}$	IRAC@Spitzer	25.0	0.2	-0.25	0.22
$4.5 \mu\text{m}$	IRAC@Spitzer	25.0	0.2	-0.25	0.22

assuming a Gaussian distribution in flux with mean and standard deviation (flux, err(flux)).

To generate the simulated catalogue, the galaxies are distributed according to  $r$ -band luminosity functions for the different spectral types. However, for simplicity in the comparison of the different codes, we do not apply any dust attenuation for the star-forming galaxies and we do not let the luminosity functions evolve with redshift. Thus, this simulated catalogue is not expected to provide a realistic distribution of low and high redshift galaxies. Note, that we do include the averaged Lyman absorption by the intergalactic medium as a function of redshift, following Madau (1995) which will affect the blue bands at high redshift. The catalogue has been cut to objects brighter than  $r = 24$ , so that only reasonably high-S/N sources are included. The redshift distribution attains a smooth shape with a peak at intermediate redshifts and few objects beyond  $z = 1.5$ .

The final catalogue consists of  $\sim 11\,000$  objects for which the redshifts are not revealed to the participants. Furthermore, a much larger training set of  $\sim 170\,000$  objects with exactly the same properties as the original catalogue is provided.

### 3.3. Results for the noise-free case

In the following we will present the results of three different template-based codes on the noise-free catalogue that were submitted after the release. The training of empirical codes on noise-free data often does not make sense. That is probably the reason why no results for empirical codes on the noise-free data have been submitted to PHAT.

The results are summarised in Fig. 4 showing the model redshift  $z_{\text{model}}$  against the redshift estimate  $z_{\text{phot}}$  and the redshift difference  $\Delta z = z_{\text{model}} - z_{\text{phot}}$ .

The ZE2-t code shows nearly perfect agreement with LP-t in this test in terms of redshift estimates. This suggests strongly that the basic interpolation of the filter- and template-curves and their subsequent convolution by the two codes leads to colour estimates that agree very well. Also the modelled attenuation of the IGM seems to be identical in both codes.

Up to a redshift of  $z \sim 2.5$  the agreement between LP-t and HY-t/BP-t is close to perfect as well. For higher redshifts there are considerable discrepancies between LP-t on the one hand and HY-t and BP-t on the other hand.

A further analysis shows that especially the blue templates with considerable UV flux get assigned grossly wrong redshift estimates. At a redshift of  $z \sim 2.5$  the Lyman- $\alpha$  line enters our filter set. These two facts suggest that the handling of the IGM, i.e. the opacity of the Lyman- $\alpha$  forest, is implemented differently in the codes. Although all codes refer to the paper of Madau (1995), it turns out that HY-t and BP-t use an analytic approximation of the opacity curve. As described in that paper the opacity curve can be approximated by a step-function with depression factors  $D_A$  and  $D_B$  shortward of Lyman- $\alpha$  and Lyman- $\beta$ , respectively, and a complete absorption shortward of the Lyman-limit. LP-t uses the full opacity curve instead (binned for redshift intervals of  $\Delta z = 0.1$ ). See Fig. 5 for a comparison of the opacity curves for a redshift of  $z = 3.5$ .

The scatter around the mean opacity curve for a given redshift is rather large (see Fig. 3 of Madau 1995) due to clustering of the IGM. Thus, for practical applications we do not expect either method to perform superior over the other one as long as a direct relation between opacity and redshift is assumed. To account for the greatly varying optical depth of the IGM for different lines-of-sight at a fixed redshift in a realistic application, one certainly would have to vary opacity as another free parameter. The discrepancies reported here just appear in this artificial test without noise and a fixed opacity-redshift relation. However, different residuals between model and observation might well be present in applications of photo- $z$  codes with a fixed opacity-redshift relation to real data.

### 3.4. Results for the catalogue with noise

We select the best fit or most likely photo- $z$  estimate from each method. Some methods provide estimates of confidence in their photo- $z$ 's in the form of redshift uncertainties or probability distributions  $P(z)$  and/or template quality of fit measurements like  $\chi^2$ . These can help identify and prune those photo- $z$  estimates most likely to be outliers. However these confidence measures are not performed consistently or universally among the various methods, so we do not consider them here.

The error distribution of photo- $z$ 's is usually non-Gaussian with extended tails and some catastrophic outliers with grossly wrong redshift estimates. To summarise this distribution by a few numbers is not always possible. Here we express the photo- $z$  accuracy in terms of the mean and the RMS scatter of the

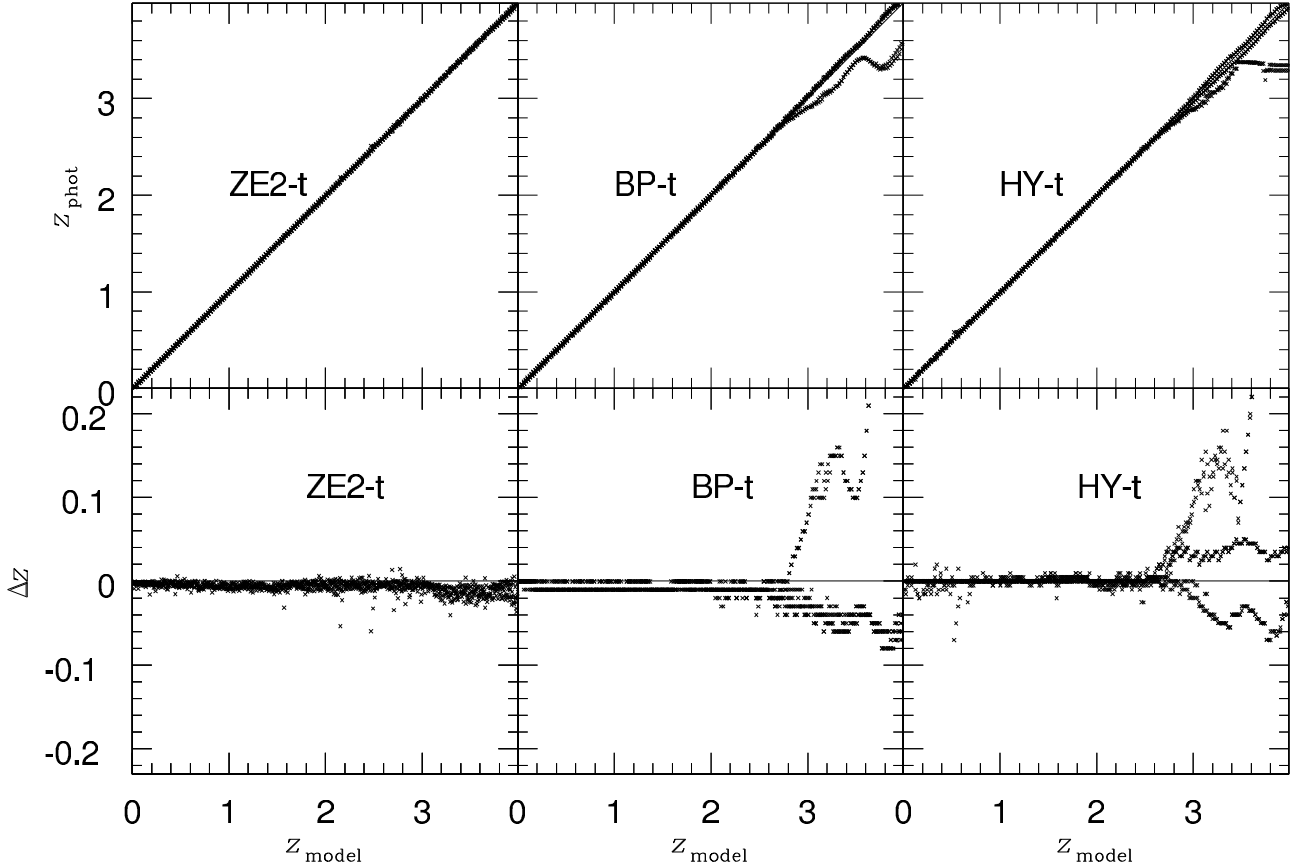


**Fig. 4.** Results of the PHAT0 test for the noise-free catalogue.

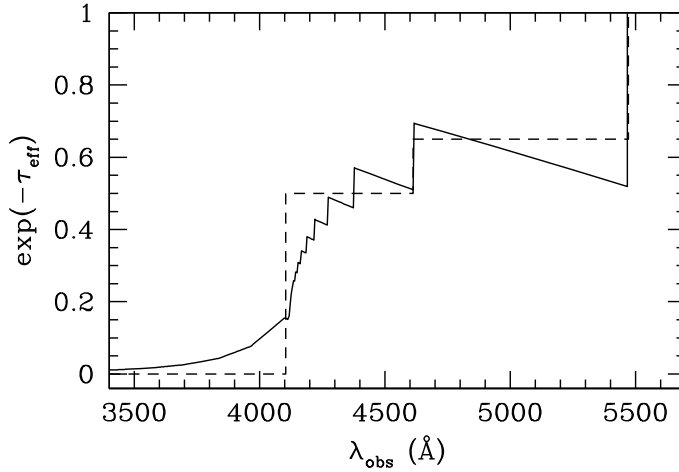


**Fig. 5.** Opacity curves used by LP-t (solid) and HY-t and BP-t (dashed) for a redshift of  $z = 3.5$ .

**Table 3.** Results for the PHAT0 catalogue with noise.

Acronym	Bias	Scatter	Outlier rate <sup>a</sup>
LP-t	0.000	0.010	0.044%
BP-t	-0.005	0.011	0.026%
EA-t	-0.001	0.012	0.000%
GA-t	0.000	0.014	0.053%
GO-t	0.000	0.012	0.018%
HY-t	-0.002	0.013	0.185%
LR-t	0.000	0.011	0.026%
PT-t	-0.005	0.011	0.053%
ZE-t	0.000	0.011	0.062%
ZE2-t	-0.005	0.011	0.044%
AN-e	0.000	0.011	0.018%
DT-e	-0.004	0.019	0.389%
PN-e	0.000	0.017	0.053%
PO-e	0.001	0.019	1.669%
RT-e	0.000	0.013	0.010%
SN-e	-0.005	0.049	18.202%

**Notes.** <sup>(a)</sup> Outliers are defined as objects with  $|\Delta z| = |z_{\text{model}} - z_{\text{phot}}| > 0.1$ .

quantity  $\Delta z = z_{\text{model}} - z_{\text{phot}}$  (after rejection of outliers), and an outlier rate, as it was done in many former studies. These statistics for the different codes can be found in Table 3. Figure 8 shows the scatter and outlier values in comparison. We define all objects with a redshift estimate that differs by more than 0.1 from the model redshift, i.e.  $|\Delta z| = |z_{\text{model}} - z_{\text{phot}}| > 0.1$ , as outliers. We refer the reader to the diagrams in Figs. 6 and 7 showing the complete error distribution.

### 3.4.1. Results from LP-t (Arnouts)

In order to set a standard to which the performance of all other codes can be compared to, we run LP-t on the catalogue with noise that was created by the code itself. It is reasonable to regard the accuracy reached by LP-t on this catalogue as a theoretical limit set by the amount of noise put in (see Sect. 3.2.4). The results are displayed in the first panels of Figs. 6 and 7 alongside the results from the other codes.

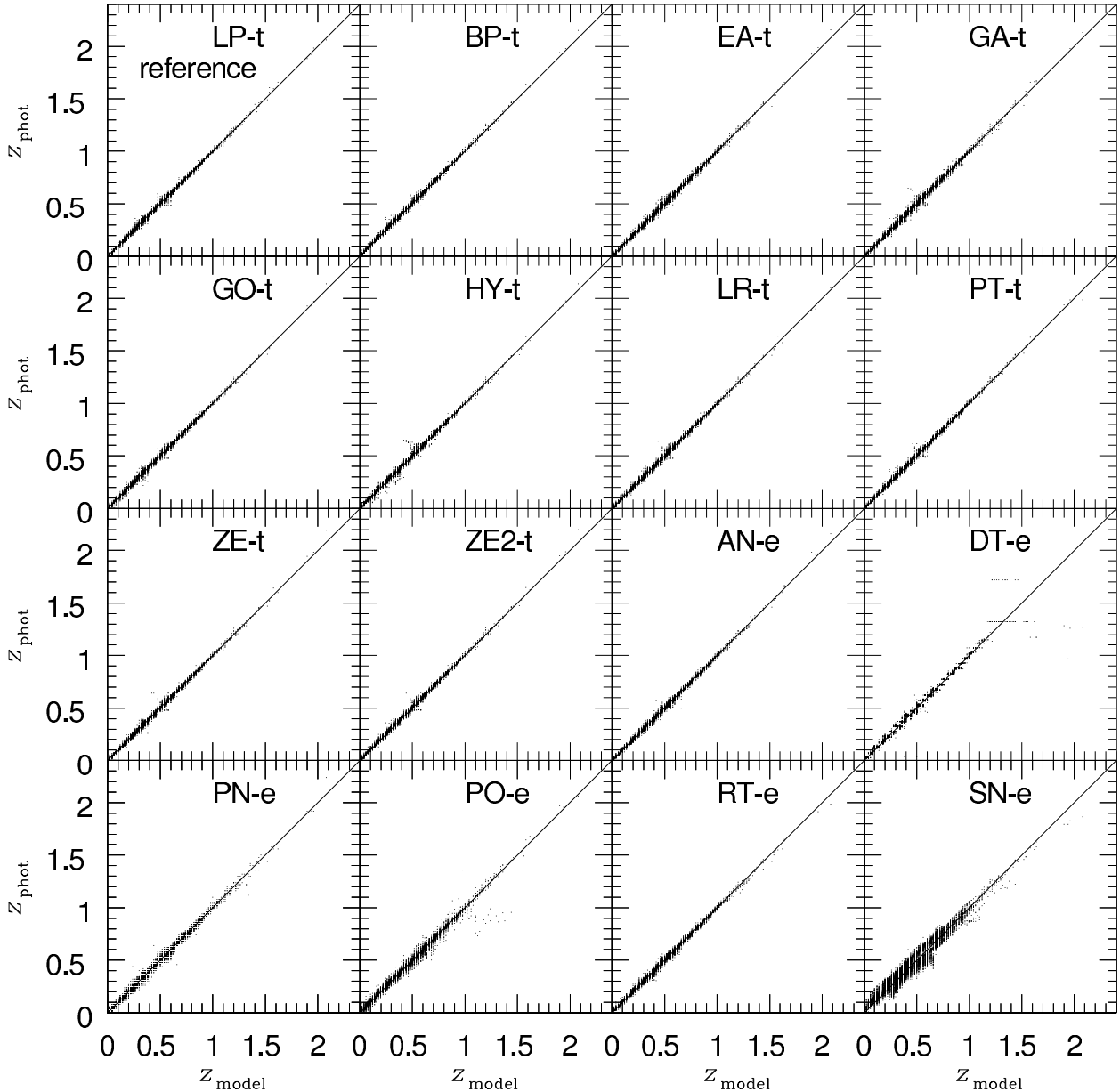


**Fig. 6.** Results of the PHAT0 test for the catalogue with noise,  $z_{\text{phot}}$  vs.  $z_{\text{model}}$ . Note that LP-t (top-left panel) was used to create the simulations and should be regarded as a reference.

### 3.4.2. Results from the other codes

The numbers in Table 3 and the observed error distributions displayed in Figs. 6 and 7 suggest that most codes tested here perform similarly to LP-t. Note that there is some degeneracy between the scatter values and the outlier rates. No significant bias is produced by any of the codes. All bias values are smaller than 0.5%. Looking at the scatter values and outlier rates four different groups can be identified:

1. a large number of codes (AN-e, BP-t, GO-t, EA-t, LR-t, RT-e, PT-t, ZE-t, ZE2-t) performs very similarly to LP-t with scatter values only slightly larger and outlier rates that are very similar or even smaller. This can be regarded as essentially identical performance because the low numbers of outliers are strongly affected by shot-noise. Note that the outlier rates of these codes correspond to 0–7 out of ~11 000 objects!

2. some other codes (GA-t, HY-t, PN-e) show larger values in both statistics than LP-t, but the differences are still minor and not very significant;
3. the codes DT-e, PO-e yield scatter values that are larger by a factor of two and outlier rates that are much larger than the LP-t statistics, with DT-e yielding a smaller outlier rate than PO-e;
4. SN-e performs worse but is still in the development phase.

In the following we discuss the problems occurring in the last two groups.

### 3.4.3. Problems

The panels for DT-e of Figs. 6 and 7 clearly show that the code performs very similar to the codes from groups 1. and 2. for redshifts  $z_{\text{model}} \lesssim 1.1$ . For larger redshifts the training set becomes more and more sparse. The division into branches of the decision

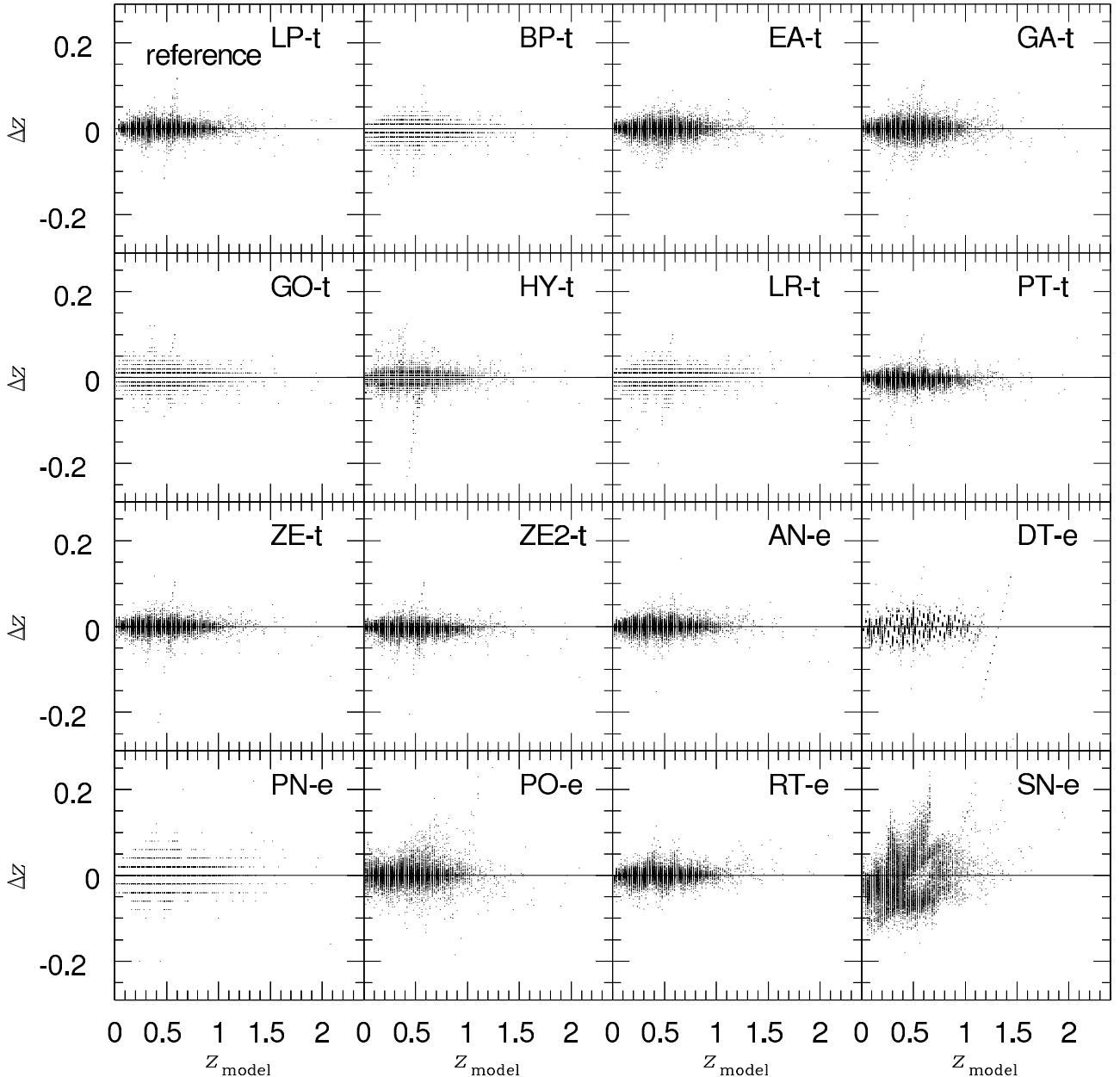


**Fig. 7.** Results of the PHAT0 test for the catalogue with noise,  $\Delta z = z_{\text{model}} - z_{\text{phot}}$  vs.  $z_{\text{model}}$ . Note that LP-t (top-left panel) was used to create the simulations and should be regarded as a reference.

tree hence becomes less precise. For the highest redshift interval only one branch is established so that objects from a rather large range in  $z_{\text{model}}$  are all assigned the same  $z_{\text{phot}}$ . This particular feature of the DT-e code leads to the slightly worse statistics reported in Table 3.

The empirical code PO-e (see Sect. 2.16) is based on a second-order polynomial fit of the colour-redshift relation. This leads to a very limited number of degrees of freedom (66 in the PHAT0 case with 11 bands) compared to the number of objects in the training set<sup>3</sup>. Not all the information included in the training set can be reflected by the 66 coefficients so that this empirical code performs worse in this test than other empirical codes (e.g. AN-e) that feature many more degrees of freedom.

The SN-e code was developed for a low redshift ( $z < 1.5$ ) dataset with robust colours and galaxy shape information, and is not currently optimised for high redshift and/or noisy data that is photometric only, as was the case with the PHAT datasets. However, it was useful to examine its unoptimised performance with the PHAT data, as an indication of the extent to which optimisation of the network characteristics to a given input data scheme matters.

## 4. PHAT1 – a test on GOODS data

### 4.1. Motivation

The estimation of photo- $z$ 's is special in the sense that the desired answer can in principle be obtained through spectroscopic observations. Thus, we have an accurate benchmark which we can compare photo- $z$ 's to and we do not have to rely fully on

<sup>3</sup> Note that PO-e was trained on a much smaller training set with  $\sim 1200$  objects.

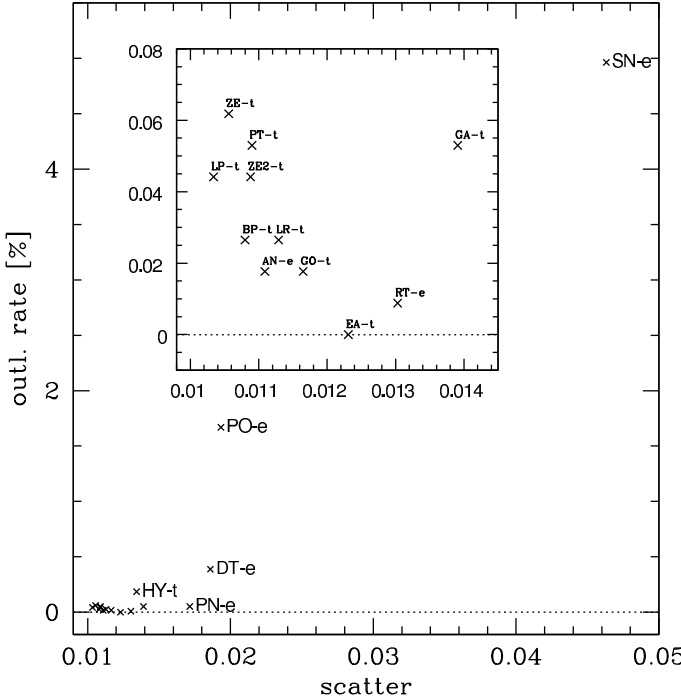


**Fig. 8.** Scatter and outlier values for the catalogue with noise of PHAT0. The inset shows the region in the lower left as a blow-up, but due to shot noise the performance of most the codes in the inset should be regarded as identical.

simulations. This is a very different situation from other estimation problems in astronomy, e.g. the estimation of shapes of galaxies for weak gravitational lensing, where accurate knowledge of the intrinsic shape is inaccessible for comparison.

Given the high complexity of the photo- $z$  approach and the multiple factors that influence the results it is reasonable to test the photo- $z$  codes on real photometric data of objects that have also been observed spectroscopically for precise redshift measurements. In this way the tendency of simulations to idealise certain aspects of real data can be avoided.

As a note of caution it should, however, be mentioned that comparisons of photo- $z$ 's to spec- $z$ 's might well draw a somewhat idealised picture of photo- $z$  performance. The currently available spectroscopic catalogues are only highly complete at bright magnitudes. For fainter magnitudes the fraction of high-quality spectroscopic redshift measurements decreases. As Hildebrandt et al. (2008) showed, the objects missing in the spec- $z$  catalogues are likely the ones for which also photo- $z$  estimation is harder and photo- $z$  accuracy is worse. We chose the GOODS-N field also for the reason that it is one of the regions of the sky with the most complete spectroscopy down to faint limits.

#### 4.2. Data set

The imaging data for this test are part of the Great Observatories Origins Deep Survey northern field (GOODS-N, Giavalisco et al. 2004). The original four-band, optical ACS data are complemented with images at other wavelengths from a variety of instruments. See Table 4 for a summary. In total, there are data in 18 bands covering the near-UV to the mid-IR.

The photometry used in the PHAT1 test is drawn from Capak et al. (2004) which includes  $U$ ,  $B_J$ ,  $V_J$ ,  $R_C$ ,  $I_C$ ,  $z'$  and

**Table 4.** Filters used for the PHAT1 test.

Filter	Instrument	$m_{\text{lim.}; \text{AB}}$
$U$	MOSAIC@KPNO-4 m	27.1 <sup>a</sup>
$B$	SUPRIMECAM@Subaru	26.9 <sup>a</sup>
$V$	SUPRIMECAM@Subaru	26.8 <sup>a</sup>
$R$	SUPRIMECAM@Subaru	26.6 <sup>a</sup>
$I$	SUPRIMECAM@Subaru	25.6 <sup>a</sup>
$Z$	SUPRIMECAM@Subaru	25.4 <sup>a</sup>
$F435W$	ACS@HST	27.8 <sup>b</sup>
$F606W$	ACS@HST	27.8 <sup>b</sup>
$F775W$	ACS@HST	27.1 <sup>b</sup>
$F850LP$	ACS@HST	26.6 <sup>b</sup>
$J$	ULBCAM@UH-2.2 m	24.1 <sup>c</sup>
$H$	ULBCAM@UH-2.2 m	23.1 <sup>c</sup>
$HK$	QUIRC@UH-2.2 m	22.1 <sup>c</sup>
$K$	WIRC@Hale-5 m	22.5 <sup>d</sup>
$3.6 \mu\text{m}$	IRAC@Spitzer	25.8 <sup>e</sup>
$4.5 \mu\text{m}$	IRAC@Spitzer	25.8 <sup>e</sup>
$5.8 \mu\text{m}$	IRAC@Spitzer	23.0 <sup>e</sup>
$8.0 \mu\text{m}$	IRAC@Spitzer	23.0 <sup>e</sup>

**Notes.** <sup>(a)</sup> 5- $\sigma$  in a circular aperture with a diameter of 3''. <sup>(b)</sup> 10- $\sigma$  in a circular aperture with a diameter of 0''.2. <sup>(c)</sup> 5- $\sigma$  for a point-source. <sup>(d)</sup> 5- $\sigma$  for a Gaussian profile with  $FWHM = 1''.3$ . <sup>(e)</sup> 10- $\sigma$  for a point-source.

$H_K'$  photometry. Deep  $J$ , and  $H$  band photometry taken with ULBCAM on the UH2.2 m (Wang et al. 2006) and  $K_s$  band photometry taken with WIRC on Palomar (Bundy et al. 2005) were added by first PSF matching then measuring photometry in 3'' diameter apertures using the method described in Capak et al. (2004). The GOODS-ACS photometry in  $F435W$  ( $B$ ),  $F606W$  ( $V+R$ ),  $F775W$  ( $i'$ ), and  $F850LP$  ( $z'$ ) along with the IRAC data (Moustakas et al. private Communication) were added by positionally matching the catalogues provided by the GOODS team with the Capak et al. (2004) catalogues using a 1'' matching radius. Following recommended practice, the SExtractor MAG\_AUTO magnitudes were used for the ACS data, while the aperture corrected 3.6'' diameter aperture magnitudes were used for IRAC.

For this stage of testing we wanted to use publicly available data that could be obtained with minimal effort by an average researcher. The results of this test illustrate the critical role that photometric methods play in obtaining good photo- $z$ 's. We strongly recommend care in obtaining photometry across images with variable and very different PSFs. Images should be aligned, the PSFs matched, and fluxes measured in consistent apertures and care should be taken to ensure noise estimates are correct (Capak et al. 2004; Capak et al. 2007; Wolf et al. 2004; Fernández-Soto et al. 2001). As illustrated by our test on one of the best studied fields in the sky, correctly measured pan-chromatic photometry is not generally available. Users will likely have to, and probably should, measure their own photometry to ensure the best results. This is made simpler by automated tasks such as ColorPro (Coe et al. 2006) which measure PSF matched aperture photometry for a combination of space and ground based data, while more complicated routines such as TFIT (Laidler et al. 2007) fit high resolution galaxy images using the local PSF for each image.

Bulk photometric offsets were removed by minimising the offset between the predicted and measured photometric points as

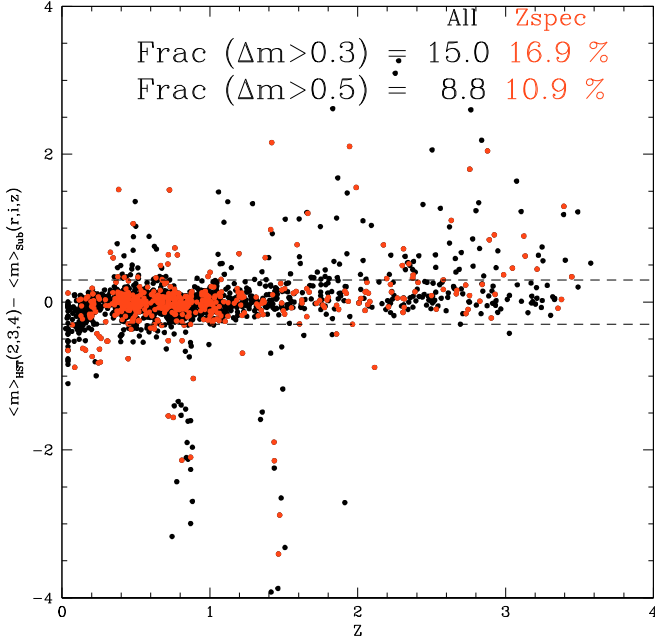


**Fig. 9.** Difference between the average ACS (mean of  $F606W$ ,  $F775W$ , and  $F850LP$ ) and average SUPRIMECAM (mean of  $R_{IZ}$ ) magnitudes as a function of redshift in the PHAT1 catalogue.

a function of rest frame magnitude as described in Capak et al. (2007)<sup>4</sup>. The resulting photometry has mean systematic offsets between photometric bands smaller than 0.01 mag. However, close inspection of the photometric catalogue shows that there is a fraction of objects which show a rather large discrepancy between the ACS- and the SUPRIMECAM-photometry in the optical. Those objects are essentially evenly distributed in redshift. A fraction of 15% (10%) of the objects shows a difference of  $>0.3$  mag ( $>0.5$  mag) between an object's average ACS magnitude (mean of  $F606W$ ,  $F775W$ , and  $F850LP$ ) and an average SUPRIMECAM magnitude (mean of  $R_{IZ}$ ), as displayed in Fig. 9. Some of these objects might be variable, while others might be affected by different blending in the space- and ground-based bands. We do not filter these objects because they are also included in photometric catalogues that are routinely used for many science projects. We want to provide estimates of photo- $z$  accuracy that are as close to reality as possible and such mismatches of photometry from different instruments (or also different bands of the same instrument) are not exceptions but rather the norm. Such issues reflect the complex problem of obtaining a good photometric catalogue from multi-band imaging data taken with different cameras and/or taken under different observing conditions. But we will comment upon the impact of these objects on global photo- $z$  performance in the following sections and mention some strategies to prune them.

The photometric catalogue is matched to different spectroscopic catalogues from Cowie et al. (2004)<sup>5</sup>, Wirth et al. (2004),

Treu et al. (2005), and Reddy et al. (2006)<sup>6</sup>. This yields a total of 1984 objects with 18-band photometry and spectroscopic redshifts. We randomly select a quarter of those objects as a training set, i.e. for the release of the catalogue the spectroscopic redshifts of one quarter of the objects are revealed<sup>7</sup>. The magnitude and redshift distributions are shown in Fig. 10. Note that the catalogue is highly complete down to  $R \sim 24$ . The PHAT1 catalogue does not only contain normal galaxies. There is a small number of AGN in the sample which we explicitly decided to include.

The participants are asked to run their codes twice on the provided catalogue, once including the IRAC bands and once without the IRAC bands. This is done because many template sets are inaccurate in the mid-IR and we do not want this effect to dominate the comparisons. Unlike in PHAT0 the participants using template-based codes were asked to choose the best possible template set for their code in PHAT1. Thus, template sets differ between the different “-t” methods here.

#### 4.3. Results for the 14-band case

We use a similar set of statistics as for the PHAT0 test to characterise the performance of the photo- $z$ 's on the PHAT1 data with two differences:

- we report the bias and scatter of  $\Delta z' = \frac{z_{\text{spec}} - z_{\text{phot}}}{1 + z_{\text{spec}}}$ ;
- outliers are defined as objects with  $|\Delta z'| > 0.15$ .

The resulting statistics are summarised in Tables 5–7<sup>8</sup> and the scatter and outlier values are plotted in Fig. 11 for the full sample and for an  $R < 24$  magnitude-limited sample. The full error distributions are displayed in Figs. 12 and 13 for the 14-band case (i.e. without the IRAC bands). The results for the empirical codes only include the non-training objects whereas the results for the template-based codes include all objects. We checked the performance of the template-based codes on the training and non-training sample and found no significant differences.

The most striking feature in Fig. 12 and Table 5 is the large fraction of outliers (>9% of the total sample) with catastrophically wrong photo- $z$ 's. This fraction is higher than typical literature estimates. It should be emphasised that some of the objects included here are unusual in the sense that they have SEDs different from normal galaxies (e.g. AGNs). A small fraction is also influenced by blending effects in the ground-based bands or variability, so that there is a mismatch between the ACS and the SUPRIMECAM optical photometry. There may also be a very small number of objects with wrong spec- $z$ 's. But the bulk of the outliers are real. If we reject objects which have discrepant photometry between ACS and SUPRIMECAM (see Sect. 4.2) the outlier rates decrease considerably as indicated by the values in brackets in Table 5. The bias is largely unaffected by this filtering and the scatter values do not decrease by more than 10% (both not given in Table 5). We also test the most accurate code in PHAT1 (LP-t) without ACS photometry. The statistics of the problematic objects do not improve significantly although

<sup>4</sup> Note that this procedure is only mildly dependent on the Capak et al. (2007) template set used for the re-calibration because the redshift range of the training sample is broad. For a given template SED the same rest frame wavelength corresponds to many different observer's frame wavelengths so that systematic features in a template get distributed evenly over many filters. Only BP-t, HY-t, and KR-t use template sets that are somewhat similar to the Capak et al. (2007) template set.

<sup>5</sup> Which includes spec- $z$ 's from Cohen et al. (1996, 2000); Cohen (2001); Phillips et al. (1997); Lowenthal et al. (1997, 1998); Dickinson (1998); Liu et al. (1999); Barger et al. (2000, 2001, 2003); Steidel et al. (1996, 2003).

<sup>6</sup> Which includes spec- $z$ 's from Blain et al. (2004).

<sup>7</sup> It should be noted that this is a fairly small training set for such a large redshift range. It cannot be expected that empirical codes perform as well on such a data set as template-based codes. This should not be regarded as a deficiency in the codes but rather a deficiency in the data.

<sup>8</sup> In Table 6 results are presented for a relaxed definition of outliers being objects with  $|\Delta z'| > 0.5$ .

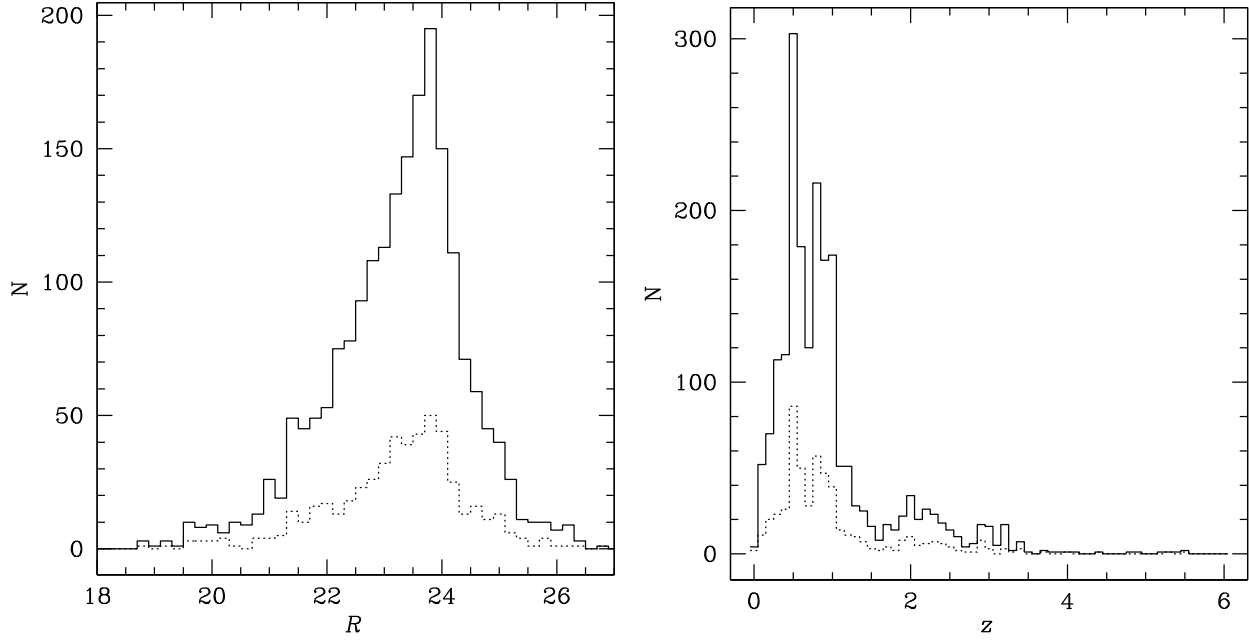


**Fig. 10.**  $R$ -band magnitude- (*left*) and redshift-distributions (*right*) of the PHAT1 catalogue (*solid*) and the training sub-sample (*dotted*).

**Table 5.** Results for the PHAT1 catalogue with and without the IRAC bands, and for all objects and a magnitude-limited sample with  $R < 24$ .

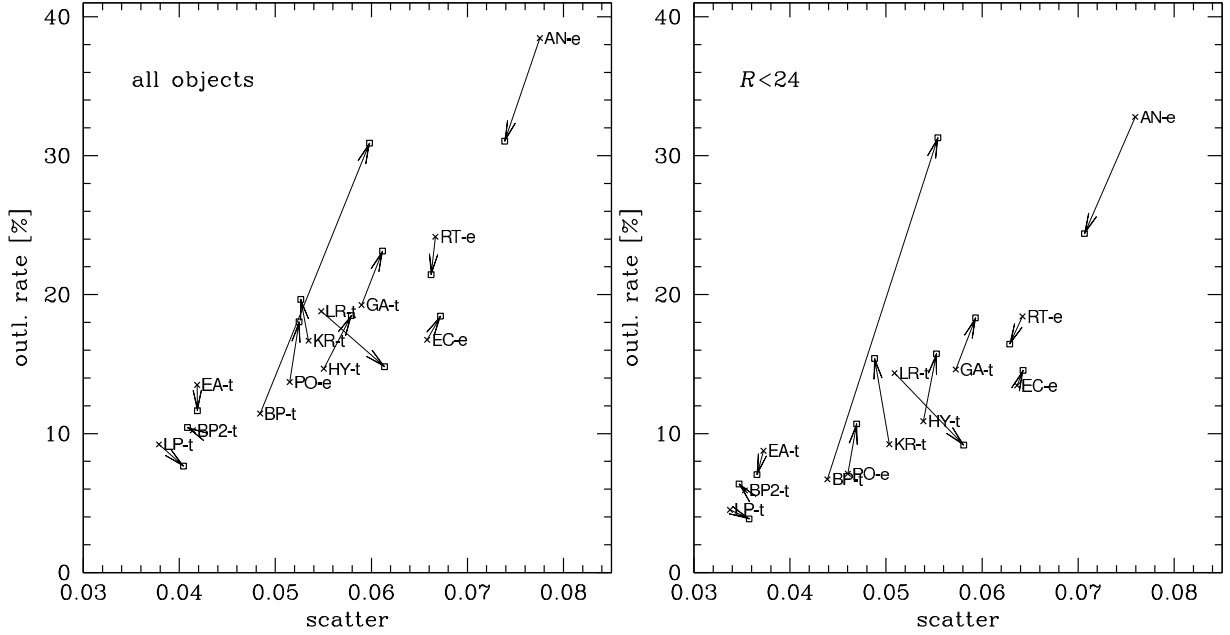
Code	18-band			14-band			18-band $R < 24$			14-band $R < 24$		
	bias	scatter	outl. <sup>a</sup>	bias	scatter	outl. <sup>a</sup>	bias	scatter	outl. <sup>a</sup>	bias	scatter	outl. <sup>a</sup>
BP-t	-0.046	0.060	30.9 (27.7)	0.011	0.048	11.4 (7.1)	-0.053	0.055	31.3	0.012	0.044	6.7
BP2-t	0.003	0.041	10.4 (7.5)	0.004	0.041	10.2 (7.8)	0.003	0.035	6.4	0.005	0.035	5.9
EA-t	0.020	0.042	11.6 (5.9)	0.022	0.042	13.5 (7.1)	0.021	0.037	7.0	0.023	0.037	8.8
GA-t	-0.009	0.061	23.1 (18.1)	0.016	0.059	19.3 (15.5)	-0.012	0.059	18.3	0.018	0.057	14.6
HY-t	-0.001	0.058	18.5 (15.2)	0.018	0.055	14.7 (10.1)	-0.002	0.055	15.7	0.019	0.054	10.9
KR-t	-0.008	0.053	19.7 (13.3)	-0.006	0.053	16.7 (9.8)	-0.010	0.049	15.4	-0.008	0.050	9.2
LP-t	0.004	0.040	7.7 (4.9)	0.009	0.038	9.2 (4.7)	0.005	0.036	3.9	0.009	0.034	4.5
LR-t	0.024	0.061	14.8 (12.9)	0.038	0.055	18.8 (15.9)	0.021	0.058	9.2	0.039	0.051	14.4
AN-e	-0.010	0.074	31.0 (29.0)	-0.006	0.078	38.5 (36.5)	-0.013	0.071	24.4	-0.007	0.076	32.8
EC-e	-0.001	0.067	18.4 (15.3)	0.002	0.066	16.7 (13.3)	-0.006	0.064	14.5	-0.003	0.064	13.5
PO-e	-0.009	0.052	18.0 (14.5)	-0.007	0.051	13.7 (9.4)	-0.009	0.047	10.7	-0.008	0.046	7.1
RT-e	-0.009	0.066	21.4 (19.0)	-0.008	0.067	24.2 (21.6)	-0.012	0.063	16.4	-0.012	0.064	18.4

**Notes.** <sup>(a)</sup> Percentage of objects with  $|\Delta z'| = \left| \frac{z_{\text{spec}} - z_{\text{phot}}}{1+z_{\text{spec}}} \right| > 0.15$ . The numbers for the cleaned sample excluding objects with discrepant ACS/SUPRIMECAM photometry are given in brackets.

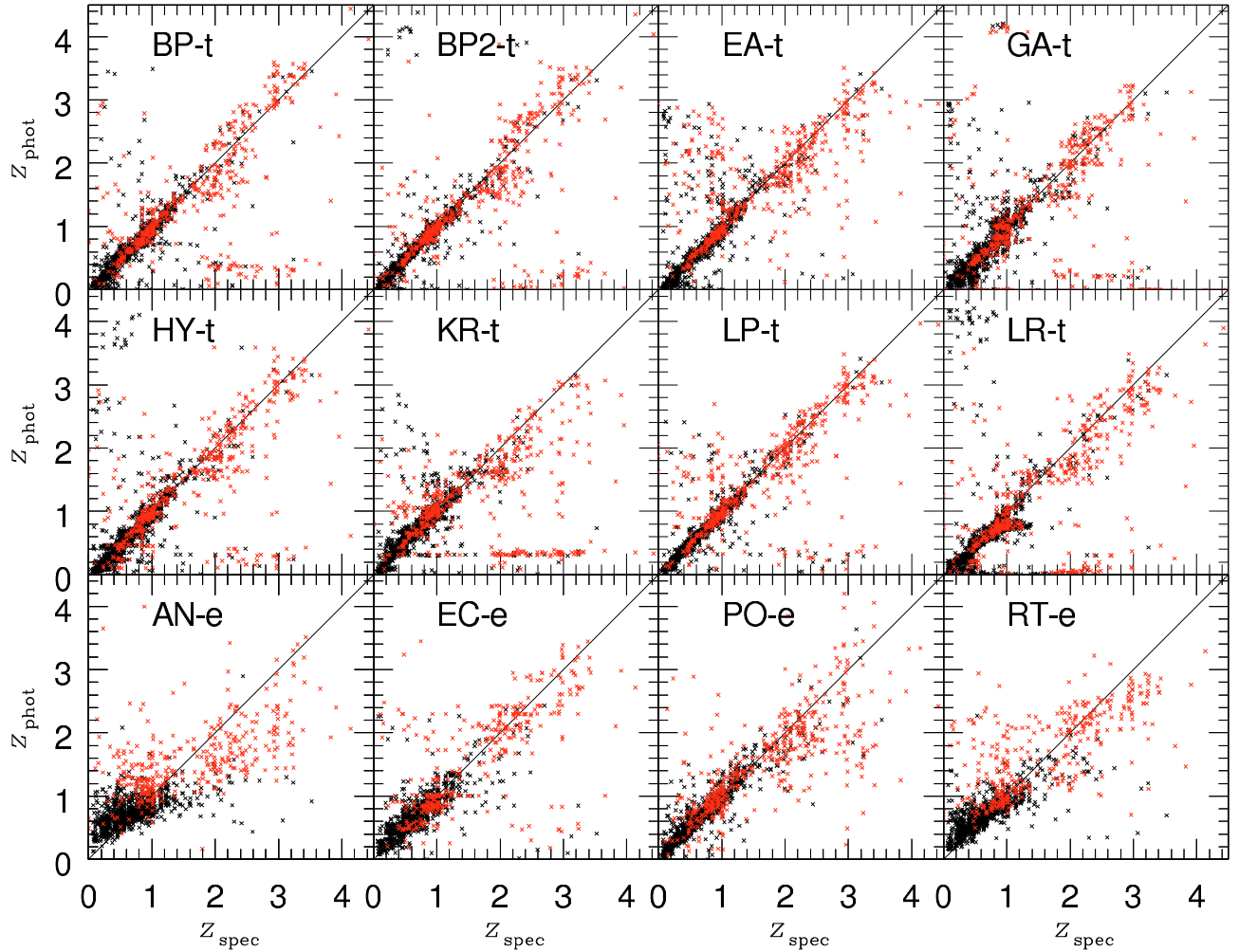
**Table 6.** Same as Table 5 but with a relaxed criterion for outliers.

Code	18-band			14-band			18-band $R < 24$			14-band $R < 24$		
	bias	scatter	outl. <sup>a</sup>	bias	scatter	outl. <sup>a</sup>	bias	scatter	outl. <sup>a</sup>	bias	scatter	outl. <sup>a</sup>
BP-t	-0.084	0.122	5.9 (5.0)	0.016	0.085	4.8 (5.0)	-0.098	0.112	5.8	-0.098	0.112	5.8
BP2-t	0.009	0.084	3.8 (2.4)	0.011	0.081	3.6 (2.4)	0.008	0.072	1.5	0.008	0.072	1.5
EA-t	0.023	0.088	4.2 (2.0)	0.026	0.092	5.5 (2.0)	0.024	0.074	1.9	0.024	0.074	1.9
GA-t	-0.014	0.125	8.7 (5.9)	0.030	0.106	7.7 (5.9)	-0.026	0.115	5.4	-0.026	0.115	5.4
HY-t	-0.011	0.116	4.9 (4.2)	0.027	0.098	4.8 (4.2)	-0.016	0.109	3.5	-0.016	0.109	3.5
KR-t	-0.015	0.114	8.6 (5.9)	-0.003	0.105	6.9 (5.9)	-0.024	0.101	6.6	-0.024	0.101	6.6
LP-t	0.003	0.079	2.3 (1.4)	0.011	0.079	3.7 (1.4)	0.005	0.060	1.0	0.005	0.060	1.0
LR-t	0.028	0.104	4.5 (4.0)	0.054	0.098	7.6 (4.0)	0.023	0.087	2.5	0.023	0.087	2.5
AN-e	-0.036	0.151	3.1 (2.4)	-0.035	0.173	4.2 (2.4)	-0.047	0.130	1.4	-0.047	0.130	1.4
EC-e	-0.007	0.120	3.6 (3.1)	-0.003	0.114	3.6 (3.1)	-0.015	0.106	1.9	-0.015	0.106	1.9
PO-e	-0.013	0.124	3.1 (2.3)	0.001	0.107	2.3 (2.3)	-0.020	0.098	1.2	-0.020	0.098	1.2
RT-e	-0.031	0.126	3.2 (2.8)	-0.028	0.137	3.6 (2.8)	-0.034	0.111	1.4	-0.034	0.111	1.4

**Notes.** <sup>(a)</sup> Percentage of objects with  $|\Delta z'| = \left| \frac{z_{\text{spec}} - z_{\text{phot}}}{1+z_{\text{spec}}} \right| > 0.5$ . The numbers for the cleaned sample excluding objects with discrepant ACS/SUPRIMECAM photometry are given in brackets.



**Fig. 11.** Scatter and outlier values for the 14- (crosses) and 18-band (squares) PHAT1 case. The arrows indicate the effect of adding the IRAC bands on photo- $z$  accuracy. The *left panel* shows the statistics for all objects and the *right panel* the ones for all objects with an  $I$ -band magnitude  $R < 24$ .

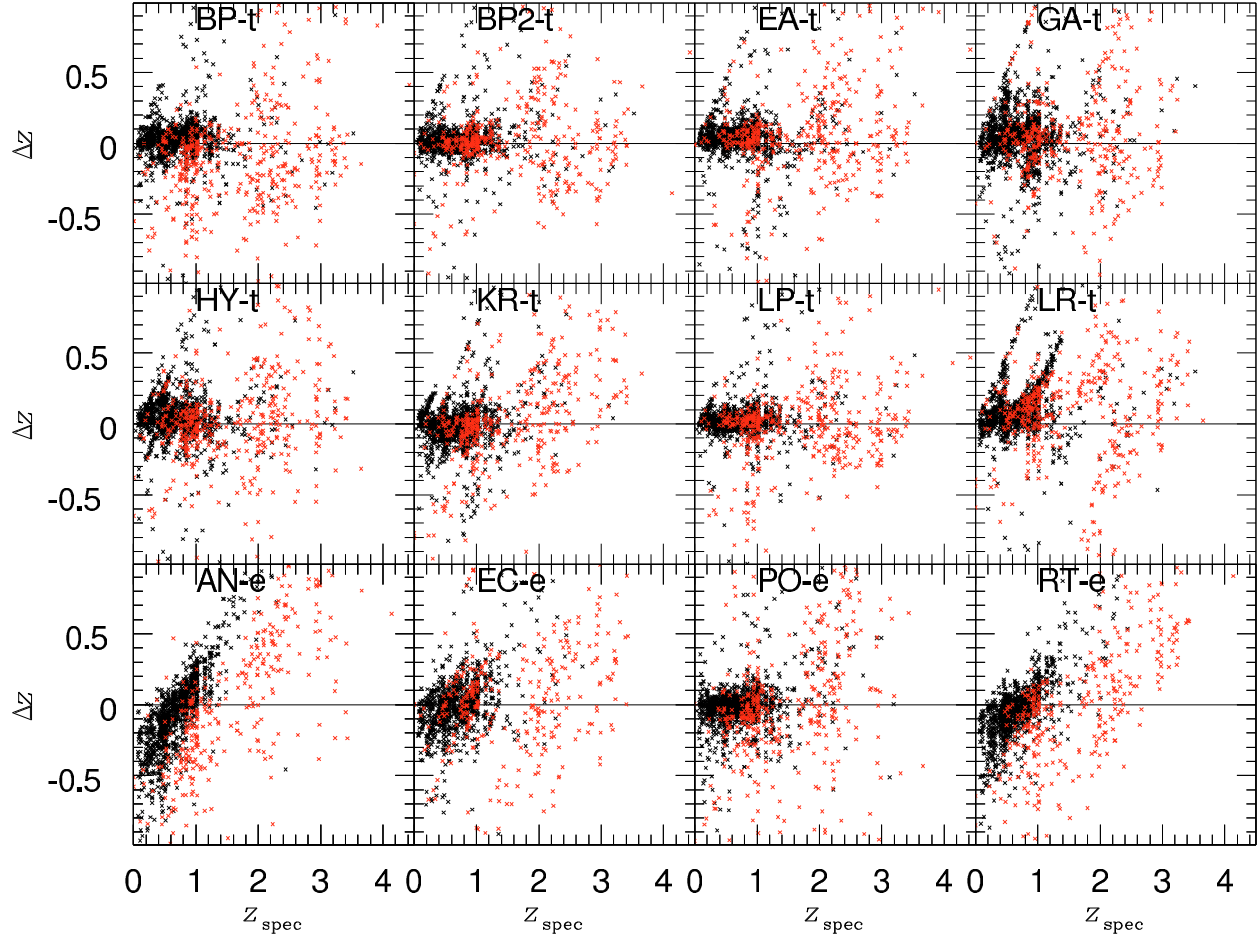


**Fig. 12.** Results of the PHAT1 test with 14 bands (i.e. excluding IRAC bands),  $z_{\text{phot}}$  vs.  $z_{\text{spec}}$ . Objects with  $R \geq 24$  are labelled in red.

**Table 7.** Same as Table 5 but in two different redshift bins.

18-band $z_{\text{spec}} \leq 1.5$			14-band $z_{\text{spec}} \leq 1.5$			18-band $z_{\text{spec}} > 1.5$			14-band $z_{\text{spec}} > 1.5$			
Code	bias	scatter	outl. <sup>a</sup>	bias	scatter	outl. <sup>a</sup>	bias	scatter	outl. <sup>a</sup>	bias	scatter	outl. <sup>a</sup>
BP-t	-0.050	0.055	31.4 (27.5)	0.013	0.044	7.2 (4.1)	-0.019	0.074	28.0 (28.9)	-0.001	0.075	35.3 (27.5)
BP2-t	0.003	0.035	6.8 (4.9)	0.005	0.035	6.5 (4.5)	0.001	0.071	30.7 (25.1)	0.001	0.075	31.0 (31.3)
EA-t	0.021	0.037	9.9 (3.9)	0.022	0.038	11.9 (4.9)	0.014	0.065	21.3 (19.9)	0.024	0.062	22.7 (22.3)
GA-t	-0.010	0.060	19.7 (14.6)	0.018	0.057	16.4 (12.9)	0.003	0.071	42.7 (42.7)	0.008	0.073	35.0 (34.1)
HY-t	-0.003	0.055	16.5 (12.9)	0.018	0.054	12.3 (8.9)	0.014	0.072	29.7 (30.8)	0.021	0.062	28.0 (18.5)
KR-t	-0.012	0.047	16.8 (11.8)	-0.011	0.050	10.5 (6.1)	0.026	0.072	35.7 (24.2)	0.042	0.062	51.3 (36.0)
LP-t	0.005	0.037	6.2 (3.2)	0.008	0.034	6.8 (2.8)	0.002	0.059	15.7 (16.6)	0.014	0.057	23.0 (18.0)
LR-t	0.023	0.059	10.1 (8.3)	0.039	0.053	15.1 (12.0)	0.028	0.079	41.3 (45.0)	0.037	0.070	39.7 (43.1)
AN-e	-0.017	0.070	27.6 (25.5)	-0.010	0.076	33.6 (31.6)	0.051	0.078	50.7 (53.2)	0.045	0.077	66.4 (70.3)
EC-e	-0.003	0.065	16.1 (12.9)	-0.000	0.064	14.5 (11.4)	0.015	0.077	32.3 (32.3)	0.015	0.077	29.5 (26.6)
PO-e	-0.012	0.049	12.6 (9.6)	-0.011	0.047	9.4 (6.0)	0.019	0.075	48.3 (48.3)	0.026	0.074	37.7 (32.7)
RT-e	-0.016	0.062	19.6 (17.0)	-0.014	0.064	21.1 (18.6)	0.040	0.072	31.8 (32.9)	0.039	0.071	41.9 (42.4)

**Notes.** <sup>(a)</sup> Percentage of objects with  $|\Delta z'| = |\frac{z_{\text{spec}} - z_{\text{phot}}}{1+z_{\text{spec}}}| > 0.15$ . The numbers for the cleaned sample excluding objects with discrepant ACS/SUPRIMECAM photometry are given in brackets.

**Fig. 13.** Similar to Fig. 12 but showing  $\Delta z = z_{\text{spec}} - z_{\text{phot}}$  vs.  $z_{\text{spec}}$ .

excluding ACS removes the discrepancy between overlapping optical filters. This suggests that most of the outliers amongst these objects are not just outliers because their photometry is corrupted, but rather because it is intrinsically harder to estimate photo- $z$ 's for them. We leave the detailed characterisation of these peculiar objects (their morphology, SEDs, remaining photometric issues, etc.) to a future study.

A lot of codes seem to have problems with identifying correctly the redshifts of objects from the Reddy et al. (2006) sample with  $1.5 \lesssim z \lesssim 3$ . We explicitly decided to include those objects in the test in order not to artificially idealise the situation. PHAT was conceived to give a realistic picture of what can be achieved with today's techniques. Those outliers reported here are present in deep photometric catalogues and it is a delicate

task for every scientist to remove those or account for their effect. The fact that literature values of outlier rates are usually smaller reflects the difficulty of a blind test, but it most probably also reflects that our combined spec- $z$  catalogue, explicitly including objects from the so-called “redshift-desert”, is more complete and representative than some other commonly used catalogues. Especially at  $R < 24$  our spec- $z$  catalogue is highly complete, and also for this bright cut the outlier rates are rather large for most codes (see Table 5 and the right panel of Fig. 11).

There are means of identifying outliers (poor fits, broad redshift-probability functions, etc.) and photometric catalogues can often be cleaned (e.g. by extraction flags) to yield much lower outlier rates. Depending on the science application such a filtering can be more or less applicable. For example, we showed that rejecting objects with problematic photometry can improve the situation considerably. However, photo- $z$ ’s are often used in a rather blind fashion without extensive checking (often due to a lack of spec- $z$  comparisons) and filtering. Some science applications also rely on redshifts for *all* objects not allowing for filtering. For those kind of applications the raw numbers reported by PHAT1 in Table 5 are more informative than the cleaned ones given in brackets.

The best performance on this data set is achieved by the LP-t, BP2-t, EA-t, and BP-t codes, with LP-t showing the smallest scatter and outlier rates. The empirical PO-e code follows closely. While EA-t and BP-t also performed nicely on the PHAT0 test with noise (LP-t was used for the creation of the PHAT0 simulations), the good results for PO-e came as a surprise because this code ranked next to last in the PHAT0 test with noise. The sparse training set of PHAT1 ( $\sim 500$  objects) is apparently large enough to fully exploit the capabilities of PO-e because there are not too many degrees of freedom involved here. In contrast, the empirical AN-e code that was in the top group for PHAT0 fails basically on PHAT1. The training set of PHAT1 is too sparse to train the neural network over this large redshift range. Neural networks are generally very good at interpolating smooth functions. However, the colour-redshift mapping of galaxies is highly complex in many places. Furthermore, there are ambiguities (also called colour-redshift degeneracies Benítez 2000) in a catalogue spanning a large redshift range, i.e. objects with very different redshifts and very similar colours. In general, neural networks, as the one used in AN-e, are not prepared to deal with such ambiguities since they only assign one output redshift to a particular point in colour space.

The top group of five (LP-t, BP2-t, EA-t, BP-t, and PO-e) is followed by HY-t, KR-t, LR-t, GA-t, EC-e, and RT-e in approximately this order. HY-t, KR-t and LR-t show some more or less pronounced, peculiar features with a number of objects being assigned very similar photo- $z$ ’s (horizontal features in Fig. 12). These features certainly have a large influence on the statistics and prevent those codes from performing as well as the top group although their error distribution in the core looks very similar. GA-t and EC-e show clearly a larger scatter in the core of the error distribution. The distribution for EC-e is smoother but with a larger width resulting in the largest scatter (excluding AN-e).

It is obvious that the empirical codes produce biases that are smaller by typically a factor of two compared to the template-based codes. The data-model match is by construction better in the empirical case. A mismatch in the template-based case can be due to both, slightly inaccurate templates and slightly inaccurate photometry. It should be noted that it is very hard to achieve a photometric cross-calibration accuracy spanning the whole wavelength range from the UV to the mid-IR. EC-e, which was designed with the goal of being as bias-free as possible, shows

by far the smallest bias indeed. The combination of a machine-learning algorithm and the proper use of PDFs pays off here.

#### 4.4. Results for the 18-band case

In Figs. 14 and 15 the results for the 18-band case (i.e. with IRAC bands included) are presented. The statistics are also listed in Table 5 and the scatter and outlier values for the different codes are plotted in Fig. 11 in comparison to the ones of the 14-band case.

It is immediately obvious, especially from Fig. 11, that not all codes benefit from adding the IRAC photometry. Only LP-t, EA-t, LR-t, RT-e, and AN-e show some improvement when adding those information about the observed-frame mid-IR SEDs of the objects. The outlier rates of LP-t and EA-t decrease by  $\sim 15\%$  compared to the 14-band case making them by far the best codes in this test, together with BP2-t, which basically shows the same performance as with 14 bands. Also RT-e improves slightly in scatter and outlier rate with 18 bands compared to 14 bands. The bias and outlier rate of LR-t are decreased somewhat but with the trade-off of a slightly larger scatter. AN-e does not perform as poorly with 18 bands as with 14 bands but is still the least accurate code in this test.

PO-e, KR-t, HY-t, GA-t, and EC-e show slightly worse performance than in the 14-band case with approximately conserved order. BP-t, however, shows a huge increase in the number of outliers by  $\sim 200\%$  due to a very poor low- $z$  performance. Most of the Coe et al. (2006) templates are undefined and must be extrapolated for  $\lambda > 25\,600 \text{ \AA}$ . These extrapolated SEDs have significantly lower fluxes in the mid-IR compared to the observed IRAC photometry resulting in a large photo- $z$  bias. Recalibration of the IRAC zeropoints with this template set improves the situation somewhat, but is not done here for simplicity. The good performance of BP2-t shows that it is not the code but the template set that makes the difference here.

#### 4.5. Discussion of the PHAT1 results

The performance shown by the best codes in the semi-blind PHAT1 test with low bias and scatter values in the 4–5% range is compatible with typical literature values. Only the large fraction of outliers ( $> 7.5\%$ ) is worse than expected. We attribute this to the higher completeness of our combined spec- $z$  catalogue besides the presence of objects with unusual SEDs and some problems with the combination of space-based and ground-based photometry. It should be noted that the PHAT1 spectroscopic catalogue represents a very deep sample and is not purely magnitude-limited. However, such depths are commonly used in photometric studies in extragalactic astronomy. We cannot fully quantify the fraction of outliers that are due to photometry problems on the one hand or due to intrinsically problematic objects with strange SEDs on the other hand. But the test of LP-t without ACS data described in Sect. 4.3 suggests that most of the problem seen here is connected to the latter.

Differences in the accuracy of the codes for the 14-band case can mostly be attributed to differences in the template sets and priors for the SED-fitting codes on the one hand and differences in the training schemes for the empirical codes on the other hand. It is not the aim of this study to explain all the features seen in this comparison. Rather we want to provide a snapshot of what current codes are capable to do in a semi-blind application.

It is striking that half of the codes perform worse with the IRAC photometry included. Especially, the low- $z$  performance

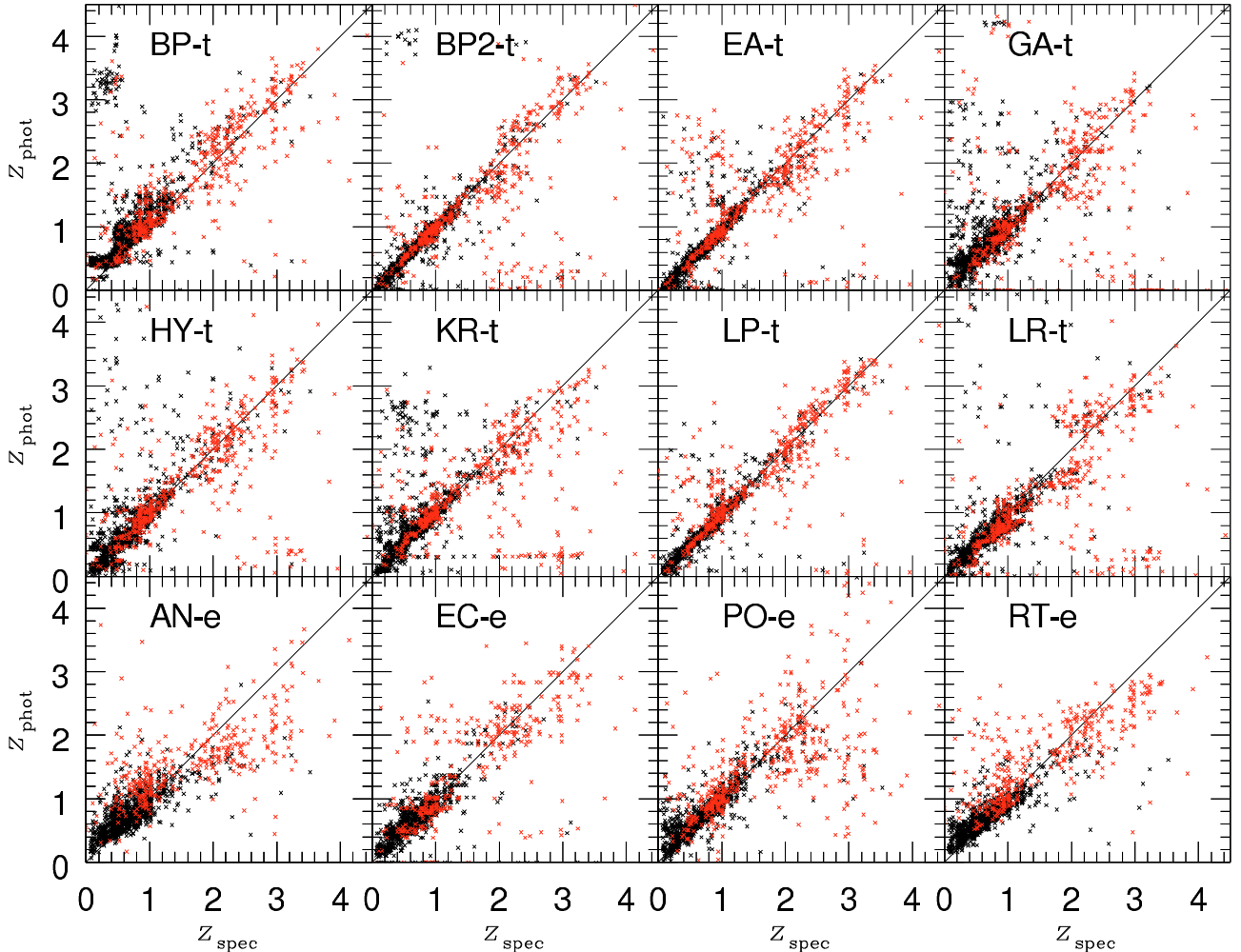


**Fig. 14.** Similar to Fig. 12 but for 18 bands (i.e. including IRAC bands).

suffers in this case. For the template-based codes this can be explained by insufficient knowledge of the template SEDs in the mid-IR<sup>9</sup>. If the templates do not represent the reality it cannot be expected that additional data lead to an improvement. EA-t, the only template-based code that really benefits from the information in the IRAC bands, differs from the other template-based codes in the sense that it uses a template error function (see Brammer et al. 2008, for a detailed description). This feature weighs the measurements in the different bands according to the estimated accuracy of the template at the rest-frame wavelength that corresponds to the effective wavelength of a given filter at a particular redshift step before computing the  $\chi^2$ . This hard-coded template error function assigns a low accuracy to the mid-IR spectral region of the templates so that the IRAC bands do not influence the  $\chi^2$  at low- $z$ . At higher redshifts, however, when IRAC probes the rest-frame near-IR or optical where templates are more accurate, the information is used and can improve the photo- $z$ 's. That is reflected in the lower bias and outlier fraction for EA-t in the 18-band case when compared to the 14-band case. BP2-t employs a filter error based on the scatter between the photometry of best-fit models and observed photometry in a particular filter on the spectroscopic training set. This essentially down-weights the IRAC bands. In general the mid-IR behaviour of the advanced template sets used by LP-t, BP2-t, and EA-t

seems to be more realistic than the extrapolations employed for some other sets leading to better performance with 18 bands.

The lower bias values produced by the empirical codes suggest that there are still systematic inaccuracies in most template sets. With a sufficient training set such inaccuracies can be repaired by re-calibrating the templates, e.g. with the approach described in Budavári et al. (2000). Such a better data-model match is demonstrated by BP2-t showing consistently the lowest bias of all template-based methods which is however still somewhat larger than the values for EC-e.

## 5. Conclusions

With PHAT we provide a snapshot of the photo- $z$  accuracy achievable with today's methods in semi-blind tests. Most major photo- $z$  codes used in the current literature are included in this challenge presented here.

A first test, PHAT0, on highly idealised simulations yields good agreement between the different codes (16 participants in total) and especially in comparison to the LP-t code that was used to create the simulations. Differences are found in the handling of the opacity of the IGM, which are most likely unimportant for practical applications (as long as only broad photometric bands are used).

The PHAT1 test based on real photometric and spectroscopic data from the GOODS survey represents a much more difficult

<sup>9</sup> This is mostly due to insufficient modelling of dust emission features from PAHs.

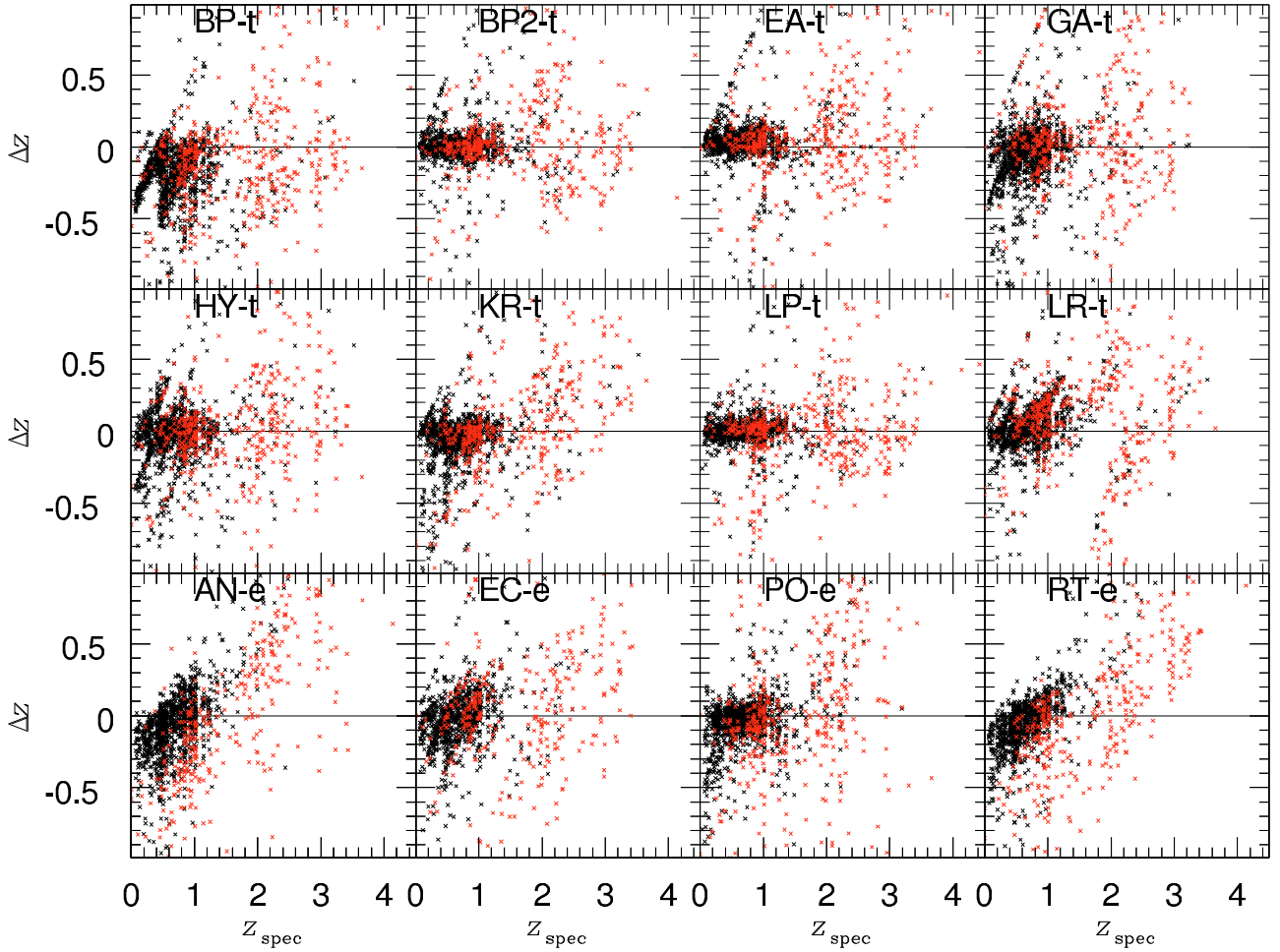


**Fig. 15.** Similar to Fig. 13 but for 18 bands (i.e. including IRAC bands).

test environment including many of the challenges encountered in practical applications. As expected the results from twelve participants show a larger fluctuation in accuracy, but a general convergence is seen for most codes, i.e. scatter values and outlier rates are within a factor of two of the best code in the test. While the best codes perform to expectations in terms of bias and scatter, some other codes show remaining biases due to a template set that does not perfectly fit the data or due to an insufficient training set. Half of the codes do not benefit from adding mid-IR photometry from the Spitzer Space Telescope. This finding suggest strongly that there is considerable inaccuracy in some of the template sets in the rest-frame mid-IR region of the SEDs. The rather large outlier rates reported in this test should be taken seriously since most of these problematic objects are also present in purely magnitude-limited photometric samples, but not necessarily in commonly used spec- $z$  catalogues, which are incomplete at fainter magnitudes. Cleaning of the catalogues is still necessary for PHAT1 to reach an outlier rate below  $\sim 5\%$  for the best code in the test. More detailed future studies (possibly in the framework of PHAT) are needed to identify the nature of this problem and quantify the contributions from multi-colour photometry issues on the one hand and objects with intrinsically unusual SEDs on the other hand. We believe that solving the problem of these outliers lies at the core of future photo- $z$  improvements. It is clear that improved spec- $z$  catalogues which are as complete as possible will be indispensable for such an effort. Some science applications that do not rely on complete samples of galaxies (like e.g. dark energy studies with weak gravitational

shear) can greatly benefit from efficient cleaning of galaxy catalogues. There are ways of considerably improving photo- $z$  accuracy by rejecting objects with unreliable estimates. It is, however, beyond the scope of this study to present strategies on how to optimise catalogues for different science applications and how to quantify those improvements.

Photo- $z$  accuracy is of paramount importance for a large number of future science projects, ranging from galaxy evolution to cosmology. The differences in the performance of the different photo- $z$  codes presented here will have a direct impact on the power of photometric surveys to answer those scientific questions. We did not quantify the impact of photo- $z$  accuracy here, but it should be noted that there is still some way to go before photo- $z$ 's reach the accuracy required for e.g. future full-sky dark energy surveys.

The test environments used in this study are publicly available at [http://www.astro.caltech.edu/twiki\\_phat/bin/view/Main/WebHome](http://www.astro.caltech.edu/twiki_phat/bin/view/Main/WebHome) and can be used to assess the performance of future methods in comparison to the results presented here in a quantitative and unbiased way.

**Acknowledgements.** We would like to thank JPL/Caltech for hospitality and support during the 2008 PHAT workshop. We are grateful to the large number of colleagues who made PHAT a success through discussions, criticism, and encouragement. A special thanks goes to Mike Hudson who came up with the acronym ‘‘PHAT’’. HH would like to thank in particular Catherine Heymans, Konrad Kuijken, Ludovic van Waerbeke, and Peter Schneider for supporting the PHAT effort. HH was supported by the European DUEL RTN, project MRTN-CT-2006-036133. The work of LAM and DC was carried out at the Jet Propulsion Laboratory, California Institute of Technology, under a contract with NASA.

LAM acknowledges support by the NASA ATPP program. CW was supported by an STFC Advanced Fellowship. NP acknowledges support from NKTH:Polanyi and KCKHA005 grants.

## References

- Abazajian, K. N., Adelman-McCarthy, J. K., Agüeros, M. A., et al. 2009, ApJS, 182, 543
- Abdalla, F. B., Amara, A., Capak, P., et al. 2008a, MNRAS, 387, 969
- Abdalla, F. B., Banerji, M., Lahav, O., & Rashkov, V. 2008b [arXiv:astro-ph/0812.3831]
- Adelman-McCarthy, J. K., Agüeros, M. A., Allam, S. S., et al. 2007, ApJS, 172, 634
- Albrecht, A., Bernstein, G., Cahn, R., et al. 2006, unpublished [arXiv:astro-ph/0609591]
- Anders, P., & Fritze, U. 2003, A&A, 401, 1063
- Arnouts, S., Moscardini, L., Vanzella, E., et al. 2002, MNRAS, 329, 355
- Assef, R. J., Kochanek, C. S., Brodwin, M., et al. 2008, ApJ, 676, 286
- Assef, R. J., Kochanek, C. S., Brodwin, M., et al. 2010, ApJ, 713, 970
- Ball, N. M., Loveday, J., Fukugita, M., et al. 2004, MNRAS, 348, 1038
- Banerji, M., Abdalla, F. B., Lahav, O., & Lin, H. 2008, MNRAS, 386, 1219
- Barger, A. J., Cowie, L. L., & Richards, E. A. 2000, AJ, 119, 2092
- Barger, A. J., Cowie, L. L., Bautz, M. W., et al. 2001, AJ, 122, 2177
- Barger, A. J., Cowie, L. L., Capak, P., et al. 2003, AJ, 126, 632
- Baum, W. A. 1962, in Problems of Extra-Galactic Research, ed. G. C. McVittie, IAU Symp., 15, 390
- Benítez, N. 2000, ApJ, 536, 571
- Benítez, N., Ford, H., Bouwens, R., et al. 2004, ApJS, 150, 1
- Blain, A. W., Chapman, S. C., Smail, I., & Ivison, R. 2004, ApJ, 611, 725
- Blanton, M. R., & Roweis, S. 2007, AJ, 133, 734
- Bolzonella, M., Miralles, J.-M., & Pelló, R. 2000, A&A, 363, 476
- Boulade, O., Charlot, X., Abbon, P., et al. 2003, ed. M. Iye, & A. F. M. Moorwood, SPIE Conf. Ser., 4841, 72
- Brammer, G. B., van Dokkum, P. G., & Coppi, P. 2008, ApJ, 686, 1503
- Bruzual , A. G., & Charlot, S. 1993, ApJ, 405, 538
- Bruzual, G., & Charlot, S. 2003, MNRAS, 344, 1000
- Budavári, T. 2009, ApJ, 695, 747
- Budavári, T., Szalay, A. S., Connolly, A. J., Csabai, I., & Dickinson, M. 2000, AJ, 120, 1588
- Bundy, K., Ellis, R. S., & Conselice, C. J. 2005, ApJ, 625, 621
- Calzetti, D., Armus, L., Bohlin, R. C., et al. 2000, ApJ, 533, 682
- Capak, P., Cowie, L. L., Hu, E. M., et al. 2004, AJ, 127, 180
- Capak, P., Aussel, H., Ajiki, M., et al. 2007, ApJS, 172, 99
- Carliles, S., Budavári, T., Heinis, S., Priebe, C., & Szalay, A. S. 2010, ApJ, 712, 511
- Coe, D., Benítez, N., Sánchez, S. F., et al. 2006, AJ, 132, 926
- Cohen, J. G. 2001, AJ, 121, 2895
- Cohen, J. G., Cowie, L. L., Hogg, D. W., et al. 1996, ApJ, 471, L5
- Cohen, J. G., Hogg, D. W., Blandford, R., et al. 2000, ApJ, 538, 29
- Coleman, G. D., Wu, C.-C., & Weedman, D. W. 1980, ApJS, 43, 393
- Collister, A. A., & Lahav, O. 2004, PASP, 116, 345
- Collister, A., Lahav, O., Blake, C., et al. 2007, MNRAS, 375, 68
- Connolly, A. J., Csabai, I., Szalay, A. S., et al. 1995, AJ, 110, 2655
- Cowie, L. L., Barger, A. J., Hu, E. M., Capak, P., & Songaila, A. 2004, AJ, 127, 3137
- Csabai, I., Budavári, T., Connolly, A. J., et al. 2003, AJ, 125, 580
- Csabai, I., Dobos, L., Trencséni, M., et al. 2007, Astron. Nachr., 328, 852
- Dahlen, T., Mobasher, B., Somerville, R. S., et al. 2005, ApJ, 631, 126
- Dahlen, T., Mobasher, B., Dickinson, M., et al. 2007, ApJ, 654, 172
- De Lucia, G., & Blaizot, J. 2007, MNRAS, 375, 2
- Dickinson, M. 1998, in The Hubble Deep Field, ed. M. Livio, S. M. Fall, & P. Madau, 219
- Fazio, G. G., Hora, J. L., Allen, L. E., et al. 2004, ApJS, 154, 10
- Feldmann, R., Carollo, C. M., Porciani, C., et al. 2006, MNRAS, 372, 565
- Fernández-Soto, A., Lanzetta, K. M., Chen, H., Pascale, S. M., & Yahata, N. 2001, ApJS, 135, 41
- Fioc, M., & Rocca-Volmerange, B. 1997, A&A, 326, 950
- Firth, A. E., Lahav, O., & Somerville, R. S. 2003, MNRAS, 339, 1195
- Gerdes, D. W., Sypniewski, A. J., McKay, T. A., et al. 2010, ApJ, 715, 823
- Giavalisco, M., Ferguson, H. C., Koekemoer, A. M., et al. 2004, ApJ, 600, L93
- Heymans, C., Van Waerbeke, L., Bacon, D., et al. 2006, MNRAS, 368, 1323
- Hildebrandt, H., Wolf, C., & Benítez, N. 2008, A&A, 480, 703
- Hogg, D. W., Cohen, J. G., Blandford, R., et al. 1998, AJ, 115, 1418
- Huterer, D., Takada, M., Bernstein, G., & Jain, B. 2006, MNRAS, 366, 101
- Ilbert, O., Arnouts, S., McCracken, H. J., et al. 2006, A&A, 457, 841
- Ilbert, O., Capak, P., Salvato, M., et al. 2009, ApJ, 690, 1236
- Jannuzzi, B. T., & Dey, A. 1999, in Photometric Redshifts and the Detection of High Redshift Galaxies, ed. R. Weymann, L. Storrie-Lombardi, M. Sawicki, & R. Brunner, ASP Conf. Ser., 191, 111
- Kennicutt, Jr., R. C. 1998, ARA&A, 36, 189
- Kinney, A. L., Calzetti, D., Bohlin, R. C., et al. 1996, ApJ, 467, 38
- Koo, D. C. 1985, AJ, 90, 418
- Kotulla, R., & Fritze, U. 2009, MNRAS, 393, L55
- Kotulla, R., Fritze, U., Weilbacher, P., & Anders, P. 2009, MNRAS, 396, 462
- Laidler, V. G., Papovich, C., Grogin, N. A., et al. 2007, PASP, 119, 1325
- Lawrence, A., Warren, S. J., Almaini, O., et al. 2007, MNRAS, 379, 1599
- Le Fèvre, O., Vettolani, G., Paltani, S., et al. 2004, A&A, 428, 1043
- Li, I. H. & Yee, H. K. C. 2008, AJ, 135, 809
- Lilly, S. J., Le Fevre, O., Crampton, D., Hammer, F., & Tresse, L. 1995, ApJ, 455, 50
- Lin, H., Kirshner, R. P., Shectman, S. A., et al. 1996, ApJ, 464, 60
- Liu, C. T., Petry, C. E., Impey, C. D., & Foltz, C. B. 1999, AJ, 118, 1912
- Loh, E. D., & Spillar, E. J. 1986, ApJ, 303, 154
- Lowenthal, J. D., Koo, D. C., Guzman, R., et al. 1997, ApJ, 481, 673
- Lowenthal, J. D., Simard, L., & Koo, D. C. 1998, in The Young Universe: Galaxy Formation and Evolution at Intermediate and High Redshift, ed. S. D'Odorico, A. Fontana, & E. Giallongo, ASP Conf. Ser., 146, 110
- Luo, B., Brandt, W. N., Xue, Y. Q., et al. 2010, ApJS, 187, 560
- Madau, P. 1995, ApJ, 441, 18
- Massey, R., Heymans, C., Bergé, J., et al. 2007, MNRAS, 376, 13
- Mobasher, B., Capak, P., Scoville, N. Z., et al. 2007, ApJS, 172, 117
- Noll, S., Mehlert, D., Appenzeller, I., et al. 2004, A&A, 418, 885
- Oesch, P. A., Carollo, C. M., Feldmann, R., et al. 2010, ApJ, 714, L47
- Onaizumi, H., Lima, M., Cunha, C. E., et al. 2008, ApJ, 674, 768
- Peacock, J. A., Schneider, P., Efstathiou, G., et al. 2006, ESA-ESO Working Group on "Fundamental Cosmology", Tech. Rep.
- Phillips, A. C., Guzman, R., Gallego, J., et al. 1997, ApJ, 489, 543
- Polletta, M., Tajer, M., Maraschi, L., et al. 2007, ApJ, 663, 81
- Prevot, M. L., Lequeux, J., Prevot, L., Maurice, E., & Rocca-Volmerange, B. 1984, A&A, 132, 389
- Puschell, J. J., Owen, F. N., & Laing, R. A. 1982, ApJ, 257, L57
- Reddy, N. A., Steidel, C. C., Erb, D. K., Shapley, A. E., & Pettini, M. 2006, ApJ, 653, 1004
- Sha, F., Lin, Y., Saul, L. K., & Lee, D. D. 2007, Neural Computation, 19, 2004
- Silva, L., Granato, G. L., Bressan, A., & Danese, L. 1998, ApJ, 509, 103
- Steidel, C. C., Adelberger, K. L., Shapley, A. E., et al. 2003, ApJ, 592, 728
- Steidel, C. C., Giavalisco, M., Dickinson, M., & Adelberger, K. L. 1996, AJ, 112, 352
- Treu, T., Ellis, R. S., Liao, T. X., & van Dokkum, P. G. 2005, ApJ, 622, L5
- Wang, W., Cowie, L. L., & Barger, A. J. 2006, ApJ, 647, 74
- Williams, R. E., Blacker, B., Dickinson, M., et al. 1996, AJ, 112, 1335
- Wirth, G. D., Willmer, C. N. A., Amico, P., et al. 2004, AJ, 127, 3121
- Wolf, C. 2009, MNRAS, 397, 520
- Wolf, C., Meisenheimer, K., Kleinheinrich, M., et al. 2004, A&A, 421, 913
- Wuyts, S., Labb  , I., Schreiber, N. M. F., et al. 2008, ApJ, 682, 985